TITLE

Sox2 and FGF20 define a temporal separation between specification and differentiation required for organ of Corti development

Lu M. Yang[1], Sung-Ho Huh[1,2,*], David M. Ornitz[1,*]

[1]Department of Developmental Biology; Washington University School of Medicine; St. Louis, Missouri, 63110; USA

[2]Holland Regenerative Medicine Program, and the Department of Neurological Sciences; University of Nebraska Medical Center; Omaha, Nebraska, 68198; USA

*Correspondence: dornitz@wustl.edu, sungho.huh@unmc.edu

ABSTRACT

The mouse organ of Corti develops in two steps: progenitor specification and differentiation. Fibroblast Growth Factor (FGF) signaling is important in this developmental pathway, as deletion of FGF receptor 1 (*Fgfr1*) or its ligand, *Fgf20*, leads to hair cell and supporting cell loss. Here, we show that while FGF20-FGFR1 signaling functions during differentiation, FGFR1 has an FGF20-independent but Sox2-dependent role in specification. We also show that decreased *Sox2* expression results in delayed specification, while loss of *Fgf20* results in premature differentiation. Thereby, *Sox2* and *Fgf20* interact to modulate a temporal buffer to ensure that specification occurs before differentiation. Consequently, loss of *Sox2* and *Fgf20* preferentially affects development of the basal end of the cochlea, which has less time separating the end of specification from the onset of differentiation. These findings reveal an intricate developmental program that regulates the precise and differential timing of organ of Corti development along the cochlea.

INTRODUCTION

The inner ear contains six sensory organs required for the senses of hearing and balance. The cochlea, a snail-like coiled duct, is the auditory organ. It contains specialized sensory epithelia, called the organ of Corti, composed of hair cells (HCs) and supporting cells (SCs). In mammals, this sensory epithelium is elegantly patterned, with one row of inner hair cells (IHCs) and three rows of outer hair cells (OHCs), separated by two rows of pillar cells forming the tunnel of Corti. Each row of OHCs is associated with a row of supporting cells called Deiters' cells. Here, we refer to pillar cells and Deiters' cells collectively as SCs.

Organ of Corti development has been described as occurring in two main steps: prosensory specification and differentiation (reviewed in Basch et al., 2015). During prosensory specification, proliferative progenitors at the floor of the developing cochlear duct are specified and exit the cell cycle to form the postmitotic prosensory domain. During differentiation, prosensory cells, bipotent progenitors that make up the prosensory domain, differentiate into both HCs and SCs (Fekete, Muthukumar, & Karagogeos, 1998). Interestingly, cell cycle exit, which marks the completion of specification, and initiation of differentiation occur in waves that travel in opposite directions along the length of the cochlear duct. At around embryonic day 12.5 (E12.5) in the mouse, progenitors begin to exit the cell cycle and express the cyclin-dependent kinase inhibitor $p27^{Kip1}$ (*Cdkn1b*) in a wave that begins at the apex of the cochlea (the cochlear tip) and reaches the base of the cochlea by around E14.5 (P. Chen & Segil, 1999; Lee, Liu, & Segil, 2006). Afterwards, the specified prosensory cells begin differentiating into HCs and SCs in a wave that begins at the mid-base at around E13.5, and spreads quickly to the rest of the base and to the apex over the next few days (reviewed in Basch et al., 2015). Notably, while the basal end of the cochlear duct differentiates immediately after prosensory specification, the apical end has a longer temporal buffer between specification and differentiation. The spiral ganglion, containing neurons synapsing to HCs, has been shown to be important for this delay in apical differentiation, via Sonic Hedgehog (SHH) signaling (Bok, Zenczak, Hwang, & Wu, 2013; Jahan, Pan, Kersigo, & Fritzsch, 2010; Matei et al., 2005; Tateya et al., 2013).

The transcription factor *Sox2* is one of the earliest markers of prosensory cells (Gu et al., 2016; Mak, Szeto, Fritzsch, & Cheah, 2009). Mice with specific *Sox2* hypomorphic mutations that affect inner ear expression have hearing impairment due to decreased HC and SC number, while mice with inner ear-specific *Sox2* null mutations are completely deaf and have no HCs or SCs (Dong et al., 2002; Kiernan et al., 2005). Genetic experiments show that *Sox2* is both

necessary and sufficient for prosensory specification. Absence of *Sox2* expression leads to the loss of *p27*^{Kip1} expression at E14, a marker for the prosensory domain (Kiernan et al., 2005), while ectopic *Sox2* expression in cochlear nonsensory epithelium can induce ectopic sensory patches (Dabdoub et al., 2008; Pan et al., 2013; Puligilla & Kelley, 2016).

The Fibroblast Growth Factor (FGF) signaling pathway also plays vital roles in organ of Corti development (reviewed in Ebeid and Huh, 2017). Studies utilizing cochlear explants showed that inhibition of FGF signaling prior to and during stages of HC and SC differentiation resulted in decreased HC and SC number (T. Hayashi, Ray, & Bermingham-McDonogh, 2008). Signaling through FGF receptor 1 (FGFR1), in particular, is essential during this process. Conditional deletion of *Fgfr1* (Fgfr1-CKO) in the developing cochlear epithelium resulted in dramatically reduced HC and SC number (Huh, Warchol, & Ornitz, 2015; Ono et al., 2014; Pirvola et al., 2002). This has been attributed to decreased *Sox2* expression in the prosensory domain of Fgfr1-CKO mice, leading to a defect in prosensory specification (Ono et al., 2014).

FGF20 has been hypothesized to be the FGFR1 ligand during organ of Corti development. Both *in vitro* inhibition of FGF20 with an anti-FGF20 antibody (T. Hayashi et al., 2008) and *in vivo* knockout of *Fgf20* (Fgf20-KO; Huh et al., 2012) led to decreased HC and SC number, similar to the Fgfr1-CKO phenotype. However, the Fgf20-KO phenotype is clearly not as severe as that of Fgfr1-CKO. Fgfr1-CKO mice are missing almost all OHCs and some IHCs (Ono et al., 2014), while Fgf20-KO mice are only missing 2/3 of OHCs and have a full complement of IHCs (Huh et al., 2012). This suggests that another FGF ligand may be redundant with and compensating for the loss of FGF20, the identity of which is currently unknown.

Another difference between Fgfr1-CKO and Fgf20-KO mice is the proposed mechanism accounting for the decrease in HCs and SCs. Interestingly, unlike in Fgfr1-CKO mice, Sox2 expression in the prosensory domain is not disrupted in Fgf20-KO mice (Huh et al., 2012; Ono et al., 2014). Rather, FGF20 seems to be involved during HC and SC differentiation. These differences between the Fgfr1-CKO and Fgf20-KO phenotypes and their relationship with *Sox2* suggest that FGF20/FGFR1 signaling has a more complex and as yet unexplained role during organ of Corti development.

Here, we hypothesize that FGFR1 signaling has functions in both steps of organ of Corti development: an earlier role in prosensory specification that involves *Sox2*, and a later role in the initiation of differentiation. We provide evidence that FGF20 regulates differentiation but not specification. We further show that *Sox2* and *Fgf20* interact to modulate the temporal buffer between prosensory specification and differentiation. As these two steps occur along a developmental pathway, we hypothesize that prosensory specification must occur prior to differentiation for sensory epithelia to develop. In *Sox2* hypomorph mice, prosensory specification is delayed, while in Fgf20-KO mice, differentiation occurs prematurely. When combined, these two defects led to differentiation attempting to initiate prior to the completion of specification, particularly at the basal end of the cochlear duct, which has a smaller temporal buffer between these two events. These results define unique functions of and complex interactions among FGF20, FGFR1, and Sox2 during organ of Corti development and highlight the importance of the timing of specification and differentiation along different regions of the cochlear duct.

RESULTS

The Fgf20-KO cochlear phenotype is less severe than the Fgfr1-CKO phenotype

Previous studies have shown that deletion of *Fgf20* leads to a loss of 2/3 of OHCs in the mouse organ of Corti (Huh et al., 2012), while conditional deletion of *Fgfr1* from the cochlear epithelium leads to a loss of almost all OHCs and some IHCs (Ono et al., 2014; Pirvola et al., 2002). To rule out the effect of genetic background accounting for these differences, we generated *Fgf20* knockout (Fgf20-KO: $Fgf20^{-/-}$) and *Fgfr1* conditional knockout (Fgfr1-CKO: $Foxg1^{Cre/+}$; $Fgfr1^{flox/-}$) mice along with litter mate controls ($Fgf20^{+/-}$ for Fgf20-KO and $Fgfr1^{flox/+}$, $Fgfr1^{flox/-}$, and $Foxg1^{Cre/+}$;$Fgfr1^{flox/+}$ for Fgfr1-CKO) on a mixed C57BL/6J and 129X1/SvJ genetic background. Fgf20-KO and Fgfr1-CKO mice were generated in separate mating. $Foxg1^{Cre}$ targets most of the otic vesicle as early as E9.5 (Hébert & McConnell, 2000) and has been used in other studies to conditionally delete *Fgfr1* (Huh et al., 2015; Ono et al., 2014; Pirvola et al., 2002). In the $Fgf20^{-}$ allele, exon 1 of *Fgf20* is replaced by a sequence encoding a GFP-Cre fusion protein (Huh et al., 2015). We also refer to this null allele as $Fgf20^{Cre}$.

We examined the cochleae at P0 (Figures 1A and 1B) and quantified the length of the cochlear duct and the number of IHCs, OHCs, and SCs (Figures 1C-1F). Refer to Figure 1—Figure supplement 1D for the positions of basal, middle, and apical turns along the cochlear duct. We identified IHCs and OHCs based on Phalloidin/p75NTR labeling, and SCs based on Prox1/Sox2 labeling (see methods). In both Fgf20-KO and Fgfr1-CKO cochleae, there were gaps in the sensory epithelium that lacked HCs and SCs along the entire cochlear duct. Quantitatively, Fgfr1-CKO cochleae had a 28% reduction in cochlear length compared to control ($Fgfr1^{Cre/+}$;$Fgfr1^{flox/+}$) cochleae, while Fgf20-KO cochleae had a 6% reduction compared to control ($Fgf20^{+/-}$). Fgfr1-CKO cochleae had a 40% reduction in the number of IHCs, while Fgf20-KO did not have a significant reduction. Fgfr1-CKO cochleae had almost a complete lack of OHCs, a 97% reduction, while Fgf20-KO cochleae only had a 76% reduction. For SCs, Fgfr1-CKO cochleae had an 84% reduction, while Fgf20-KO cochleae had a 59% reduction. These patterns persisted when HC and SC numbers were normalized to cochlear length. These results were all expected based on previous studies (Huh et al., 2012; Ono et al., 2014) and showed that the Fgfr1-CKO phenotype is more severe than the Fgf20-KO phenotype in cochlear length and in the number of HCs and SCs. We hypothesize that during organ of Corti development, an additional FGFR1 ligand compensates for the loss of FGF20 (Figure 1G).

Notably, while the total number of IHCs was decreased in Fgfr1-CKO cochleae, the decrease was only observed in the basal and middle turns of the cochlea, not in the apical turn (Figure 1—Figure supplement 1A). In addition, the number of IHCs normalized to cochlear length was slightly increased in Fgf20-KO cochleae (Figure 1D), and this increase was only prominent in the middle and apical turns of the cochlea, but not in the basal turn (Figure 1—Figure supplement 1A). The increase in IHCs could be explained by the shortened cochlear duct length in Fgf20-KO mice. No such basal/middle/apical turn discrepancies existed in the number of OHCs or SCs in either genotype (Figure 1—Figure supplement 1B and 1C).

FGFR1 regulates *Sox2* expression while FGF20 does not

Next, we examined *Sox2* expression in Fgf20-KO and Fgfr1-CKO cochleae at E14.5 by RNA in situ hybridization and immunofluorescence. In control cochleae, *Sox2* mRNA and protein were highly expressed in the prosensory domain (Figure 2A, refer to Figure 2B). The expression of *Sox2* was not changed in Fgf20-KO cochleae compared to control; however, it was noticeably

decreased in Fgfr1-CKO cochleae (Figure 2A), in agreement with previous findings (Huh et al., 2012; Ono et al., 2014; Pirvola et al., 2002). This indicates that FGFR1 has an additional role, independent of FGF20, in regulating *Sox2*, which is required for prosensory specification (Kiernan et al., 2005). We hypothesize that another FGF ligand signaling via FGFR1 regulates *Sox2* expression during prosensory specification, while FGF20 signaling via FGFR1 regulates differentiation (Figure 2C).

We also wanted to confirm that FGF20 signals to epithelial FGFR1 at around the initiation of differentiation. To do so, we examined the expression of *Etv4* (also known as *Pea3*) and *Etv5* (also known as *Erm*), two well-established downstream effectors of FGF signaling (Ornitz & Itoh, 2015), by in situ hybridization. The expression of these two genes have been shown to be downregulated with FGF signaling inhibition in E14 cochlear explants (T. Hayashi et al., 2008). At E14.5, there were two domains of *Etv4* and *Etv5* expression in control cochleae: one in the prosensory domain, and one in the outer sulcus (Figure 2—Figure supplement 1A, brackets). The outer sulcus is the region of the cochlear epithelium abneural to the prosensory domain at E14.5. In Fgf20-KO cochleae, expression of both genes was completely absent from the prosensory domain. In Fgfr1-CKO cochleae, expression of both genes was similarly absent from the prosensory domain. Expression of *Etv4* and *Etv5* in the outer sulcus was not affected in either Fgf20-KO or Fgfr1-CKO cochleae (Figure 2-Figure supplement 1A). These results confirm that FGF20 signals through epithelial FGFR1.

Previous studies have also reported a decrease in proliferation in the Kölliker's organ (neural to the prosensory domain, Figure 2—Figure supplement 1B) in Fgfr1-CKO cochleae (Pirvola et al., 2002). We replicated this result by examining EdU (5-ethynyl-2'-deoxyuridine) incorporation at E14.5. *Fgfr1*-CKO mice had a complete lack of EdU-incorporating Kölliker's organ cells, while Fgf20-KO mice did not show a decrease in EdU incorporation (Figure 2—Figure supplement 1B). This finding is consistent with an additional FGF ligand signaling via FGFR1, likely at an earlier stage. We do not know whether the proliferation defect in the Kölliker's organ contributes to the reduction in HC and SC number in Fgfr1-CKO mice.

Genetic rescue of the Fgf20-KO phenotype suggests that FGF20 is required for differentiation

We have previously shown that recombinant FGF9, which is biochemically similar to FGF20 (Ornitz & Itoh, 2015; Zhang et al., 2006), is able to rescue the loss of HCs and SCs in Fgf20-KO explant cochleae (Huh et al., 2012). Interestingly, while treatment with FGF9 at E13.5 and E14.5 was able to rescue the Fgf20-KO phenotype, treatment at E15.5 was not. This temporal rescue specificity suggests that FGF20 signaling is required for the initiation of HC and SC differentiation.

To confirm the hypothesis that FGF20 is involved in differentiation and not specification (Figure 2C), we sought to more accurately determine the temporal requirement of FGF20 signaling. To achieve this, we developed an *in vivo* genetic rescue model of the Fgf20-KO phenotype by ectopically expressing FGF9. We combined $Fgf20^{Cre}$ with the $Fgf20^{\beta gal}$ (Huh et al., 2012), $ROSA^{rtTA}$ (Belteki et al., 2005) and TRE-Fgf9-IRES-eGfp (White et al., 2006) alleles to generate Fgf20-rescue ($Fgf20^{Cre/\beta gal}$;$ROSA^{rtTA/+}$;TRE-Fgf9-IRES-eGfp) mice along with littermate controls: Fgf20-het ($Fgf20^{Cre/+}$;$ROSA^{rtTA}$), Fgf9-OA ($Fgf20^{Cre/+}$;$ROSA^{rtTA/+}$;TRE-Fgf9-IRES-eGfp), and Fgf20-null ($Fgf20^{Cre/\beta gal}$;$ROSA^{rtTA}$). These mice express the reverse tetracycline transactivator (rtTA) in the $Fgf20^{Cre}$ lineage, which contains the prosensory domain and the Kölliker's organ at E13.5 to E15.5 (Huh et al., 2015). In mice expressing TRE-Fgf9-IRES-eGfp, rtTA drives the

expression of FGF9 upon doxycycline (Dox) induction. The *Fgf20*$^{\beta gal}$ allele is another *Fgf20*-null allele, in which exon 1 of *Fgf20* is replaced by a sequence encoding β-galactosidase. We combined *Fgf20*^{Cre} with *Fgf20*$^{\beta gal}$ to generate homozygous mutant mice to maintain a constant dosage of *Fgf20*^{Cre} in control and knockouts.

Initially, pregnant dams were fed a Dox diet from E13.5 to E15.5 and pups were harvested at P0 to examine HC and SC development. As expected, Dox treatment itself did not appear to affect HC or SC development in Fgf20-het and Fgf20-null cochleae, both of which showed the expected phenotypes (Figures 3A and 3B). Ectopic expression of FGF9 during these stages also did not affect HC or SC development in Fgf9-OA cochleae, showing that excess FGF20/FGF9 was not sufficient to produce ectopic HCs and SCs. Notably, ectopic expression of FGF9 resulted in a full rescue of the number and patterning of HCs and SCs in Fgf20-rescue pups. The organ of Corti in these rescue pups had one row of IHCs, three rows of OHCs, and five rows of SCs throughout the entire length of the cochlear duct, without any gaps (Figures 3A and 3B). This shows that FGF20/FGF9 signaling at E13.5-E15.5 is sufficient for HC and SC differentiation. The quantified results from all of the rescue experiments are summarized in Figure 3C, where the number of OHCs and SCs are represented as a percentage of that of Fgf20-het mice treated with the same Dox regimen. Raw quantified data are in Figure 3—Figure supplement 1.

To more precisely determine the timing of rescue sufficiency, we fed pregnant dams Dox for a period of 24 hours starting at E13.5, E14.5, or E15.5. With E13.5 Dox, patterning and OHC number in the basal turn of the cochlea were completely rescued (Figure 3A). However, OHC number in the middle and particularly the apical turns were only partially rescued, resulting in regions with two rows of OHCs instead of three. For instance, in the apical turn, OHC number was restored to 81% of Fgf20-het mice, which is statistically significantly increased compared to Fgf20-null, but also statistically significantly decreased compared to Fgf20-het, indicating partial rescue (Figure 3C). With E14.5 Dox, patterning and OHC number in the middle and apical turns were completely rescued. However, OHC number in the basal turn was not completely rescued, with regions of one or two rows of OHCs, instead of three. With E15.5 Dox, patterning and OHC number was not rescued in the basal and middle turns, as gaps still formed between islands of HCs (Figure 3A). However, OHC number in the apical turn was partially rescued, with two or three rows of OHCs not separated by gaps towards the tip of the apex. In all of these experiments, the rescue of SCs followed the same pattern as that of OHCs (Figure 3B).

These rescue results show that FGF20/FGF9 is sufficient for OHC and SC differentiation in the basal turn of the cochlea at E13.5, in the middle and apical turns at E14.5-E15.5, and in the tip of the apical turn at E15.5. Since the initiation of HC and SC differentiation occurs in the base/mid-base of the cochlea at E13.5 and progresses apically over the next few days, these results strongly imply that FGF20 functions during the initiation of differentiation, rather than prosensory specification, consistent with our model (Figure 2C).

Decrease in *Sox2* expression results in similar phenotypes as disruptions to FGFR1 signaling

Our results and previous findings suggest that FGFR1 regulates prosensory specification via *Sox2* (Ono et al., 2014). Mice with an inner ear-specific *Sox2* hypomorphic mutation (*Sox2*$^{Ysb/Ysb}$, see below) have defects in prosensory specification, accounting for a small loss of HCs and SCs, whereas mice with inner-ear specific *Sox2* null mutations have a complete lack of prosensory specification and a complete absence of sensory epithelium (Kiernan et al., 2005).

To examine how much the reduction in *Sox2* expression in Fgfr1-CKO cochlea contributes to the phenotype at P0, we combined the *Sox2*$^{-}$ (*Sox2* constitutive null) and *Sox2*^{Ysb} alleles to closely examine the effects of reduction in *Sox2* expression on organ of Corti development, on a similar genetic background as our Fgf20-KO and Fgfr1-CKO mice. We hypothesized that if *Fgfr1* acts upstream of *Sox2*, then reducing *Sox2* expression should at least partially recapitulate the Fgfr1-CKO cochlea phenotype. The *Sox2*^{Ysb} allele has an insertion in chromosome 3, resulting in hypomorphic *Sox2* expression in the inner ear (Dong et al., 2002; Kiernan et al., 2005).

We generated *Sox2*$^{+/+}$ (wildtype), *Sox2*$^{Ysb/+}$, *Sox2*$^{Ysb/Ysb}$, and *Sox2*$^{Ysb/-}$ mice. In this allelic series, decrease in *Sox2* expression had a dose-dependent effect on cochlea length at P0 (Figures 4A-4C). *Sox2*$^{Ysb/+}$ cochleae had a 6% reduction in length compared to wildtype (although not statistically significant), *Sox2*$^{Ysb/Ysb}$ cochleae had a 24% reduction, and *Sox2*$^{Ysb/-}$ had a 46% reduction. *Sox2*$^{Ysb/+}$ organ of Corti developed relatively normally, with three rows of OHCs and one row of IHCs (Figure 4A). Interestingly, there were occasional ectopic IHCs medial (neural) to the normal row of IHCs, especially in the middle and apical turns of the *Sox2*$^{Ysb/+}$ cochlea (Figure 4A, arrowheads). However, there was no significant increase in IHC number (total or normalized to length) compared to wildtype cochleae (Figure 4D). The *Sox2*$^{Ysb/Ysb}$ cochlea appeared much more abnormal, with gaps in the sensory epithelium that lacked HCs and SCs in the basal turn (Figures 4A and 4B), similar to what was observed previously (Kiernan et al., 2005). Moreover, at the base, in the sensory islands between the gaps, there were often four rows of OHCs and six rows of SCs. In the middle and apical turns, there were the normal three rows of OHCs and five rows of SCs. There were also numerous ectopic IHCs throughout the middle and apical turns, sometimes forming an entire second row of cells (Figure 4A), resulting in increased number of IHCs in the middle turn compared to wildtype (Figure 4—Figure supplement 1A). However, the total and length-normalized number of IHCs in *Sox2*$^{Ysb/Ysb}$ cochleae did not significantly differ from that of wildtype cochleae (Figure 4D). In terms of OHCs, *Sox2*$^{Ysb/Ysb}$ cochleae exhibited a 40% decrease in total number compared to wildtype cochleae (Figure 4E). This decrease was not quite as severe when normalized to cochlear length (21% decrease). Strikingly, *Sox2*$^{Ysb/-}$ cochleae lacked almost all HCs and SCs, except in the apical turn (Figures 4A and 4B). The decrease in OHC number (93%) in *Sox2*$^{Ysb/-}$ cochleae compared to wildtype was more severe than the decrease in IHC number (75%). Notably, IHC number was significantly decreased in the basal and middle turns, but not in the apical turn (Figure 4—Figure supplement 1A). OHC number was significantly decreased throughout all three turns (Figure 4—Figure supplement 1B). In all of these genotypes, the number of SCs followed the pattern of loss of OHCs (Figures 4F and Figure supplement 1C).

Overall, these results showed that the basal end of the cochlea is more sensitive to the loss of *Sox2* expression than the apical end. Furthermore, while both IHCs and OHCs were affected, OHCs were more sensitive to decrease in *Sox2* expression than IHCs. Importantly, both of these features were found in Fgfr1-CKO cochleae, where the decrease in IHCs was only found in the basal and middle turns and there were almost no OHCs along the entire cochlear duct (Figures 1A, 1D, 1E and Figure supplement 1A-1C). Therefore, we conclude that decrease in *Sox2* expression, leading to defects in prosensory specification, could account for the Fgfr1-CKO phenotype. Furthermore, the decrease in *Sox2* expression could also account for the difference in severity between the Fgfr1-CKO and Fgf20-KO phenotypes, since Fgf20-KO cochleae, which had normal *Sox2* expression, did not have a decrease in the number of IHCs, unlike Fgfr1-CKO and *Sox2*$^{Ysb/-}$ cochleae.

Decrease in levels of Sox2 expression delays prosensory specification

We sought to determine why a decrease in *Sox2* expression more severely affected the basal end of the cochlear duct. Initially, we examined *Sox2* expression at E14.5. As expected, Sox2 expression was almost completely absent in *Sox2*$^{Ysb/-}$ cochleae (Figure 5—Figure supplement 1A). This decrease was not more severe at the basal turn of the cochlear duct, relative to the middle and apical turns, suggesting that the more severe basal phenotype in *Sox2*$^{Ysb/-}$ cochleae cannot be explained by differential Sox2 expression.

As described in the introduction, waves of cell cycle exit (marking the completion of prosensory specification) and initiation of differentiation travel in opposite directions along the cochlear duct during development, resulting in the basal end of the cochlear duct differentiating immediately after specification. The apical end, meanwhile, exhibits a delay in differentiation, resulting in a longer temporal buffer between specification and differentiation. In this developmental pathway, specification must be completed prior to the initiation of differentiation. We reasoned, therefore, that disruptions to the timing of prosensory specification will preferentially interfere with basal sensory epithelia development.

To test this hypothesis, we examined cell cycle exit in the prosensory domain via Ki67 expression as a marker of the status of specification. Ki67 is expressed by cycling cells, but not cells in G_0 (Scholzen & Gerdes, 2000). In the developing cochlea at around E12.5 to E15.5, cells of the prosensory domain, sometimes referred to as the zone of non-proliferation, have turned off or are beginning to turn off Ki67 (P. Chen & Segil, 1999). At E14.5 in *Sox2*$^{Ysb/+}$ cochleae, the prosensory domain along most of the cochlear duct (serial sections 2-6) has turned off Ki67 expression, except at the very base (serial section 1; Figure 5A, brackets). See Figure 5—Figure supplement 1B for serial “mid-modiolar” sections through the cochlea. This indicates that the wave of cell cycle exit, which starts at the apex, has reached the very base of the cochlear duct. However, in *Sox2*$^{Ysb/-}$ cochleae, only the prosensory domain at the apical turn of the cochlear duct (serial section 6) has turned off Ki67, not the mid-basal or basal turns (serial sections 1-3); the middle turns (serial sections 4 and 5), meanwhile, were just starting to turn off Ki67 (Figure 5A, brackets). This indicates that cell cycle exit has only reached the middle turn, suggesting a delay in prosensory specification. In addition, the nuclei of prosensory domain cells shift away from the luminal surface of the cochlear epithelium upon specification (Kelley, 2007). This basal shift of nuclei localization within the cell leaves a blank space between DAPI-stained nuclei and the luminal surface of the cochlear duct, which can be visualized in all six serial sections in *Sox2*$^{Ysb/+}$ cochleae at E14.5 (Figure 5A, asterisks). However, in *Sox2*$^{Ysb/-}$ cochleae, cells of the prosensory domain mostly did not exhibit this nuclei shift at E14.5.

At E15.5, the prosensory domain along the entire length of the cochlear duct has turned off Ki67 expression in both *Sox2*$^{Ysb/+}$ and *Sox2*$^{Ysb/-}$ cochleae (Figure 5A, brackets), indicating that prosensory specification in *Sox2*$^{Ysb/-}$ cochleae has caught up by this stage. Prosensory nuclei localization has also begun to catch up at E15.5 in *Sox2*$^{Ysb/-}$ cochleae (Figure 5A, asterisks). Overall, these results suggest that prosensory specification is delayed in *Sox2*$^{Ysb/-}$ cochleae, but not permanently disrupted.

We hypothesize that prosensory specification must occur prior to differentiation to generate HCs and SCs. Therefore, the period of time in between cell cycle exit and the initiation of differentiation represents a temporal buffer (Figure 5B, green shading) preventing differentiation from occurring prior to specification. As differentiation begins in the basal/mid-basal cochlear turns shortly after specification, the delay in specification in *Sox2*$^{Ysb/-}$ cochleae leads to

progenitors not having been specified in time for differentiation at the basal end of the cochlear duct (Figure 5B, crosshatch pattern). We propose that this explains why the basal end of the cochlea is more sensitive to decreases in the level of *Sox2* expression.

Sox2* is upstream of *Fgf20

While the delay in prosensory specification can explain the preferential loss of sensory epithelium from the basal end of *Sox2* hypomorph cochleae, it does not readily explain the preferential loss of OHCs, relative to IHCs. Since this preference for OHC loss is reminiscent of the *Fgf20*/*Fgfr1* deletion phenotypes, we investigated the possibility that *Sox2* may be upstream of FGF20-FGFR1 signaling. Interestingly, both *Etv4* and *Etv5* were dramatically downregulated in the prosensory domain of $Sox2^{Ysb/-}$ cochleae compared to control (Figure 6A). This shows that FGF20-FGFR1 signaling was disrupted in the *Sox2* hypomorph cochleae. Examination of *Fgfr1* and *Fgf20* expression by in situ hybridization revealed that while *Fgfr1* expression did not appear to be affected in $Sox2^{Ysb/-}$ cochleae at E14.5, *Fgf20* expression was absent (Figure 6B). This suggests that while *Fgfr1* functions upstream of *Sox2*, *Fgf20* is downstream of *Sox2*. This model predicts that *Fgf20* expression would be downregulated in Fgfr1-CKO cochleae, which was confirmed by in situ hybridization (Figure 6C).

The above results indicate that the loss of *Fgf20* could partially account for the $Sox2^{Ysb/-}$ phenotype. To determine whether loss of *Fgf20* also causes delayed prosensory specification, we examined Ki67 expression in Fgf20-KO cochleae. At E14.5, there was no detectable delay in cell cycle exit in Fgf20-KO cochleae, as loss of Ki67 expression reached the base (serial section 1) in both control and Fgf20-KO cochleae (Figure 6D, brackets). See Figure 6—Figure supplement 1A for serial “mid-modiolar” sections through the cochlea. There was also no detectable delay in basal nuclei shift in Fgf20-KO cochleae (Figure 6D, asterisks). These results were expected as the Fgf20-KO phenotype is not more severe at the basal end of the cochlear duct. This is also consistent with *Fgf20* being required during differentiation rather than prosensory specification (Figure 6E). However, these results do not answer whether and how the loss of *Fgf20* contributes to the *Sox2* hypomorph phenotype.

We also wanted to investigate whether decrease in *Sox2* expression can account for the absence of proliferation in the Kölliker’s organ of Fgfr1-CKO cochleae. Interestingly, EdU-incorporation was decreased in the Kölliker’s organ in $Sox2^{Ysb/-}$ cochleae at E14.5, especially in the region adjacent to the prosensory domain (Figure 6—Figure supplement 1B, bracket). However, EdU-incorporation was not completely absent from the Kölliker’s organ, unlike in Fgfr1-CKO cochleae. This suggests that loss of *Sox2* in combination with other factors contribute to the Kölliker’s organ phenotype in Fgfr1-CKO cochleae.

***Sox2* and *Fgf20* interact during cochlea development**

To explore whether and how the loss of *Fgf20* contributes to the *Sox2* hypomorph phenotype, we combined the $Fgf20^{-}$ and $Sox2^{Ysb}$ alleles to remove *Fgf20* in the less severe *Sox2* hypomorphic background. We also hypothesized that reducing *Sox2* expression in $Fgf20^{-/-}$ mice would recapitulate (or phenocopy) the more severe Fgfr1-CKO phenotype, in which FGF20 signaling is lost in addition to a decrease *Sox2* expression. We interbred F1 mice from the same parents to generate nine different F2 genotypes encompassing all possible combinations of the $Fgf20^{-}$ and $Sox2^{Ysb}$ alleles: $Fgf20^{+/+}$;$Sox2^{+/+}$, $Fgf20^{+/+}$;$Sox2^{Ysb/+}$, $Fgf20^{+/-}$;$Sox2^{+/+}$, $Fgf20^{+/-}$;$Sox2^{Ysb/+}$, $Fgf20^{+/+}$;$Sox2^{Ysb/Ysb}$, $Fgf20^{+/-}$;$Sox2^{Ysb/Ysb}$, $Fgf20^{-/-}$;$Sox2^{+/+}$, $Fgf20^{-/-}$;$Sox2^{Ysb/+}$, and $Fgf20^{-/-}$;$Sox2^{Ysb/Ysb}$ (Figures 7A and 7B and data not shown). At P0, an overview of HCs and

SCs showed that the *Fgf20*$^{+/-}$;*Sox2*$^{Ysb/-}$ phenotype mostly resembled that of *Fgf20*$^{+/+}$;*Sox2*$^{+/+}$, *Fgf20*$^{+/+}$;*Sox2*$^{Ysb/+}$, and *Fgf20*$^{+/-}$;*Sox2*$^{+/+}$ cochleae, except for the prevalence of ectopic IHCs (Figure 7A, arrowheads). The *Fgf20*$^{+/-}$;*Sox2*$^{Ysb/Ysb}$ phenotype mostly resembled that of *Fgf20*$^{+/+}$;*Sox2*$^{Ysb/Ysb}$ cochleae, but with more gaps in the basal cochlear turn and two rows of IHCs throughout the length of the cochlear duct, except where there were gaps. The *Fgf20*$^{-/-}$;*Sox2*$^{Ysb/+}$ phenotype mostly resembled that of *Fgf20*$^{-/-}$;*Sox2*$^{+/+}$ cochleae, but with smaller sensory islands in between gaps. The *Fgf20*$^{-/-}$;*Sox2*$^{Ysb/Ysb}$ phenotype appeared by far the most severe, with almost a complete absence of IHCs, OHCs, and SCs from the basal turn, and tiny sensory islands in the middle turn; however, the apical turn appeared similar to that of *Fgf20*$^{-/-}$;*Sox2*$^{Ysb/+}$ and *Fgf20*$^{-/-}$;*Sox2*$^{+/+}$ cochleae (Figures 7A and 7B).

Quantification of the phenotypes are presented in Figures 7D-7G and Figure supplement 1B-1D. We analyzed the quantified P0 phenotype via two-way ANOVA with the gene dosage of *Fgf20* (levels: *Fgf20*$^{+/+}$, *Fgf20*$^{+/-}$, *Fgf20*$^{-/-}$) and *Sox2* (levels: *Sox2*$^{+/+}$, *Sox2*$^{Ysb/+}$, *Sox2*$^{Ysb/Ysb}$) as the two factors. Results from the two-way ANOVA and post-hoc Tukey's HSD are presented in Figures 7C, 7H, and Figure supplement 1A and 1E. Cochlear length and the total number of IHCs, OHCs, and SCs were all significantly affected by both the *Fgf20* dosage and the *Sox2* dosage, as well as an interaction between the two factors (Figures 7C-7G). The statistically significant interaction between *Fgf20* and *Sox2* dosages suggests that *Fgf20* and *Sox2* have a genetic interaction. Notably, *Fgf20*$^{+/-}$;*Sox2*$^{Ysb/Ysb}$ cochleae had significantly fewer OHCs and SCs than *Fgf20*$^{+/+}$;*Sox2*$^{Ysb/Ysb}$ cochleae, and *Fgf20*$^{-/-}$;*Sox2*$^{Ysb/+}$ cochleae had significantly fewer OHCs than *Fgf20*$^{-/-}$;*Sox2*$^{+/+}$ cochleae. Importantly, *Fgf20*$^{-/-}$;*Sox2*$^{Ysb/Ysb}$ cochleae had decreased total and length-normalized number of IHCs, which was not observed in any of the other genotypes, strongly supporting a genetic interaction between *Fgf20* and *Sox2* (*Fgf20*$^{+/+}$;*Sox2*$^{Ysb/Ysb}$ cochleae did have a slight decrease in the total number IHCs, but not in the length-normalized number of IHCs).

Interestingly, while the total number of IHCs was decreased in *Fgf20*$^{-/-}$;*Sox2*$^{Ysb/Ysb}$ cochleae relative to all other genotypes, this decrease was only found in the basal and middle turns, but not the apical turn (Figure 7—Figure supplement 1B and 1E). No such basal/middle/apical turn discrepancies existed in the number of OHCs or SCs (Figure 7—Figure supplement 1C-1E). This is reminiscent of the Fgfr1-CKO and *Sox2*$^{Ysb/-}$ phenotypes.

To ensure that the *Fgf20*$^{-}$ and *Sox2*^{Ysb} interaction is not purely an artifact of the *Sox2*^{Ysb} allele, we generated *Fgf20*$^{+/+}$;*Sox2*$^{+/+}$ (wildtype), *Fgf20*$^{+/-}$;*Sox2*$^{+/+}$ (Fgf20-het), *Fgf20*$^{+/+}$;*Sox2*$^{+/-}$ (Sox2-het), and *Fgf20*$^{+/-}$;*Sox2*$^{+/-}$ (double het) mice to look for an epistatic interaction between the *Fgf20*$^{-}$ and *Sox2*$^{-}$ alleles (Figure 7—Figure supplement 2A). At P0, cochlear length did not significantly differ among the four genotypes (Figure 7—Figure supplement 2B). HC quantification showed that neither *Fgf20* nor *Sox2* exhibited haploinsufficiency for total or length-normalized number of IHCs or OHCs (Figure 7—Figure supplement 2C and 2D). However, in Fgf20-het and much more so in Sox2-het cochleae, occasional ectopic IHCs can be found in the middle and apical turns of the cochlear duct (Figure 7—Figure supplement 2A, arrowheads). Interestingly, in double het cochleae, many more ectopic IHCs were found, even in the basal turn. These ectopic IHCs led to an increase in the total and length-normalized number of IHCs in double het cochleae, compared to wildtype (Figure 7—Figure supplement 2C). Notably, a significant increase in IHCs was only found in the basal turn, not the middle or apical turns (Figure 7—Figure supplement 2E). In the basal turn, IHC number was significantly increased in double het cochleae compared to wildtype, Fgf20-het, and Sox2-het. Double het cochleae also had a significant decrease in total and length-normalized number of OHCs compared to wildtype (Figure 7—Figure supplement 2D). Again, a significant decrease in OHCs

was only found in the basal turn, not the middle or apical turns (Figure 7—Figure supplement 2F). These results confirm a genetic epistatic interaction between *Fgf20* and *Sox2*.

Fgf20-KO organ of Corti exhibits premature differentiation

We propose that the *Fgf20*$^{-/-}$;*Sox2*$^{Ysb/Ysb}$ phenotype lies in between that of Fgfr1-CKO and *Sox2*$^{Ysb/-}$ in terms of severity of reductions in cochlear length and in the number of HCs and SCs. We further hypothesize that these three phenotypes form a continuum with the Fgf20-KO phenotype (Figure 8A). Along this continuum, all four genotypes lack FGF20 signaling, but vary in the level of *Sox2* expression and phenotype severity in the basal end of the cochlear duct and the outer compartment (outer rows of OHCs and SCs). From this, and from the *Fgf20*$^{-}$ and *Sox2*^{Ysb} series of alleles, we conclude that the basal end of the cochlear duct and the outer compartment are more sensitive to the loss of *Fgf20* and *Sox2*, relative to the apical end and inner compartment, respectively.

To determine what is mediating the *Sox2* and *Fgf20* interaction, we asked whether the similarity between the *Fgf20*$^{-/-}$;*Sox2*$^{Ysb/Ysb}$ and *Sox2*$^{Ysb/-}$ phenotypes could be explained by a further decrease in *Sox2* levels in *Fgf20*$^{-/-}$;*Sox2*$^{Ysb/Ysb}$ cochleae from *Sox2*$^{Ysb/Ysb}$ levels. In other words, we asked whether loss of *Fgf20* further reduces *Sox2* expression on a *Sox2* hypomorphic background. Examination of prosensory domain *Sox2* expression at E14.5 revealed, as expected, that *Fgf20*$^{-/-}$;*Sox2*$^{Ysb/+}$ cochleae did not have a decrease in Sox2 expression compared to *Fgf20*$^{+/-}$;*Sox2*$^{Ysb/+}$ (Figure 8—Figure supplement 1A). *Fgf20*$^{-/-}$;*Sox2*$^{Ysb/Ysb}$ cochleae also did not have a further decrease in Sox2 expression compared to *Fgf20*$^{+/-}$;*Sox2*$^{Ysb/Ysb}$ cochleae. Moreover, despite the loss of sensory epithelium in most of the basal turn, Sox2 expression was not further decreased in the basal turn at E14.5 relative to the rest of the *Fgf20*$^{-/-}$;*Sox2*$^{Ysb/Ysb}$ cochlea (Figure 8—Figure supplement 1A). These data confirm that *Fgf20* does not regulate *Sox2* expression.

Next, we asked whether *Sox2* and *Fgf20* interact to delay prosensory specification. We showed that Fgf20-KO cochleae do not have a delay in prosensory specification (Figure 6D). However, this does not rule out the possibility that the loss of *Fgf20* on a *Sox2* hypomorphic background may contribute to a delay. We examined Ki67 expression at E14.5 and found that in *Fgf20*$^{+/-}$;*Sox2*$^{Ysb/+}$ cochleae, prosensory domain cell cycle exit has reached the end of the base (serial section 1; Figure 8B, brackets). See Figure 8—Figure supplement 1B for serial “mid-modiolar” sections through the cochlea. Similarly, cell cycle exit in *Fgf20*$^{-/-}$;*Sox2*$^{Ysb/+}$ cochleae also reached the very base. As expected, *Fgf20*$^{+/-}$;*Sox2*$^{Ysb/Ysb}$ cochleae exhibited a slight delay in prosensory specification; cell cycle exit has reached the base (serial section 2), but has not yet reached the end of the base (serial section 1). Importantly, *Fgf20*$^{-/-}$;*Sox2*$^{Ysb/Ysb}$ cochleae did not show a further delay relative to *Fgf20*$^{+/-}$;*Sox2*$^{Ysb/Ysb}$. There was also no detectable delay in basal nuclei shift in *Fgf20*$^{-/-}$;*Sox2*$^{Ysb/+}$ or *Fgf20*$^{-/-}$;*Sox2*$^{Ysb/Ysb}$ cochleae (Figure 8B, asterisks). These results suggest that the loss of *Fgf20* does not contribute to delayed specification and that the severity of the *Fgf20*$^{-/-}$;*Sox2*$^{Ysb/Ysb}$ basal phenotype cannot be completely attributed to delayed specification.

We showed that *Fgf20* likely plays a role during the initiation of differentiation. Previous studies showed that deletion of both transcription factors *Hey1* and *Hey2* results in premature differentiation in the organ of Corti (Benito-Gonzalez & Doetzlhofer, 2014). Furthermore, it has been suggested that FGF signaling, in particular FGF20, regulates *Hey1* and *Hey2* expression during this process (Benito-Gonzalez & Doetzlhofer, 2014; Tateya et al., 2013). To test whether *Fgf20* is upstream of *Hey1* and *Hey2*, we looked at the expression of the two transcription factors via in situ hybridization. In Fgf20-KO cochleae at E14.5, *Hey1* expression is

downregulated while *Hey2* is almost completely absent compared to control (Figure 8C). To test whether this leads to premature differentiation in Fgf20-KO cochleae, we examined myosin VI (Myo6) expression, a marker of differentiated HCs (Benito-Gonzalez & Doetzlhofer, 2014). In control cochleae at E14.5, no Myo6-expressing cells were found in serial sections through the cochleae in all five embryos examined (0/5); however, in Fgf20-KO cochleae, Myo6-expressing HCs were found in several serial sections in the mid-basal and basal turns of the cochleae in four out of five embryos examined (4/5; Figure 8D). In one Fgf20-KO embryo, Myo6-expressing HCs were found up to the mid-apical turn of the cochlea (not shown). These results show that there is premature differentiation in Fgf20-KO cochleae.

Similar to a delay in prosensory specification, premature differentiation narrows the temporal buffer between the completion of specification and initiation of differentiation. In the context of a slight delay in specification due to decreased *Sox2* levels, premature differentiation from the loss of *Fgf20* can lead to an attempt at differentiation before specification, particularly in the basal end of the cochlea. We conclude that *Sox2* and *Fgf20* interact to regulate the boundaries of the temporal buffer, ensuring that differentiation begins after the completion of specification (Figure 9).

Lastly, we examined proliferation in the *Fgf20*$^{-}$ and *Sox2*^{Ysb} E14.5 cochleae. Interestingly, there was a noticeable decrease in the number of EdU-incorporating cells in Kölliker's organ in *Fgf20*$^{-/-}$;*Sox2*$^{Ysb/Ysb}$ cochleae, compared to *Fgf20*$^{+/-}$;*Sox2*$^{Ysb/+}$, *Fgf20*$^{-/-}$;*Sox2*$^{Ysb/+}$, and *Fgf20*$^{+/-}$;*Sox2*$^{Ysb/Ysb}$ cochleae (Figure 8—Figure supplement 1C). This phenotype is similar to that of *Sox2*$^{Ysb/-}$ cochleae and is less severe than that of Fgfr1-CKO cochleae. These findings suggest that *Fgf20* and *Sox2* interact to regulate proliferation in the Kölliker's organ, although other factors downstream of *Fgfr1* also contribute.

DISCUSSION

Fgfr1 is involved in prosensory specification and differentiation, while *Fgf20* is only involved in differentiation

Fgf20 and *Fgfr1* are required for HC and SC development. Based on similarities in the phenotype caused by the loss of FGF20 and loss of FGFR1 signaling, FGF20 has been hypothesized as the FGFR1 ligand during organ of Corti development (T. Hayashi et al., 2008; Huh et al., 2012, 2015; Ono et al., 2014; Pirvola et al., 2002). However, the exact role of FGF20/FGFR1 during organ of Corti development has been a topic of debate. We previously reported that *Fgf20*-null mice do not have defects in prosensory specification, and have a normally formed prosensory domain (Huh et al., 2012). We further showed that FGF20 signaling is important during the initiation stage of differentiation, and that mice lacking *Fgf20* have gaps in the differentiated sensory epithelium filled with undifferentiated prosensory progenitors. However, other studies have shown *in vitro* that FGF20 regulates prosensory specification via *Sox2* (Munnamalai, Hayashi, & Bermingham-McDonogh, 2012) and *in vivo* that *Fgfr1* is required for prosensory specification via *Sox2* (Ono et al., 2014). Here, using an *in vivo* rescue model, we show that ectopic FGF9 signaling is sufficient to rescue the *Fgf20*-null phenotype in a spatiotemporal pattern that matched the timing of differentiation along the length of the cochlear duct. We conclude, therefore, that FGF20 is involved in differentiation and not in prosensory specification.

Notably, the *Fgf20*-null phenotype, in which two-thirds of OHCs fail to develop, is not as severe as the *Fgfr1*-conditional null phenotype, which lacks almost all OHCs as well as half of IHCs.

Potential explanations for this include differences in mouse genetic background, and the existence of another redundant FGF ligand(s). To rule out the former, we examined here *Fgf20*-null and *Fgfr1*-conditional null mice on a similar genetic background, and replicated the difference in phenotype severity. We also replicated the decrease in *Sox2* expression in the prosensory domain previously reported in *Fgfr1*-conditional null mice (Ono et al., 2014). We further reaffirmed that *Sox2* expression in the prosensory domain is not affected by the loss of *Fgf20*. This suggests that another FGF ligand signaling through FGFR1 is required to maintain *Sox2* expression during prosensory specification. The identity of this ligand is currently unknown.

Foxg1^{Cre} has been used in several studies to target the otic epithelium, including to conditionally delete *Fgfr1* (Huh et al., 2015; Ono et al., 2014; Pirvola et al., 2002). One concern with *Foxg1*^{Cre} is that it is a null allele (Hébert & McConnell, 2000). *Foxg1*-null mice have shortened cochlear length, although HC and SC differentiation did not appear to be directly affected (Pauley, Lai, & Fritzsch, 2006). Previous studies (Brown & Epstein, 2011) and our results here showed that *Foxg1* is not haploinsufficient during cochlea development, as *Foxg1*$^{Cre/+}$;*Fgfr1*$^{flox/+}$ cochleae had very similar phenotypes to *Fgfr1*$^{+/-}$ cochleae. Moreover, the use of the Six1enh21-Cre transgene, which targets the otic epithelium in a similar spatiotemporal pattern as *Foxg1*^{Cre}, to conditionally delete *Fgfr1* resulted in the same phenotype as *Foxg1*$^{Cre/+}$;*Fgfr1*$^{flox/-}$ cochleae (Ono et al., 2014). This included the loss of almost all OHCs, loss of IHCs, and decreased prosensory *Sox2* expression. Therefore, the increased severity of *Foxg1*$^{Cre/+}$;*Fgfr1*$^{flox/-}$ cochleae relative to *Fgf20*$^{-/-}$ cochleae is likely not attributable *Foxg1* haploinsufficiency.

We hypothesized that the severity of the *Fgfr1*-conditional null phenotype is due to the loss of FGF20 signaling during differentiation and decreased *Sox2* expression causing disrupted prosensory specification. Consistent with this hypothesis, the combination of *Fgf20*$^{-/-}$ and *Sox2*$^{Ysb/Ysb}$ mutations phenocopied *Fgfr1* conditional null cochleae. The similarities in phenotype include approximately a 30% reduction in cochlear length and almost a complete loss of OHCs and SCs and approximately a 50% loss of IHCs. Interestingly, the *Fgf20*$^{-/-}$;*Sox2*$^{Ysb/Ysb}$ phenotype is also similar to the *Sox2*$^{Ysb/-}$ phenotype. We conclude that the *Fgfr1* conditional null, *Fgf20*$^{-/-}$;*Sox2*$^{Ysb/Ysb}$, and *Sox2*$^{Ysb/-}$ phenotypes likely lie along the same continuum, as these three genotypes all exhibited a lack of *Fgf20* expression or signaling and varying levels of *Sox2* expression (Figure 7D). *Fgf20*-null cochleae, in which *Sox2* expression was not affected, lies at the mild end of this continuum. Interestingly, this continuum shows that in the absence of *Fgf20* expression or signaling, reductions in the level of *Sox2* most severely affected sensory epithelium development of the cochlear base and the outer compartment. Moving from the *Fgf20*$^{-/-}$ (mild) end of the spectrum towards the *Sox2*$^{Ysb/-}$ (severe) end, increasing numbers of HCs and SCs are lost, preferentially form the cochlear base and the outer compartment.

***Sox2* and *Fgf20* interact to modulate a temporal buffer between specification and differentiation**

We show here conclusive evidence that *Fgf20* and *Sox2* have a strong genetic interaction during cochlea development. While we hypothesize that *Sox2* and *Fgf20* are involved in distinct steps during organ of Corti development (prosensory specification and differentiation, respectively), there is nevertheless potential for a strong interaction. We propose that the timing of specification and differentiation define a temporal buffer preventing differentiation from initiating prior to the completion of specification, and that *Sox2* and *Fgf20* interact to modulate the borders of this buffer. In a developmental pathway, the upstream event (specification) must occur prior to the downstream event (differentiation). Therefore, loss of *Sox2* and *Fgf20* leading

to delayed specification and premature differentiation, respectively, disrupts the temporal buffer. This disruption particularly affects development towards the basal end of the cochlear duct, where the buffer is the narrowest (Figure 9). We further show that the cochlear base is also sensitive to slight perturbations in *Sox2* and *Fgf20*, as the loss of a copy of each gene leads to hair cell defects in the base. The sensitivity of the cochlear base to genetic perturbations of *Sox2* and *Fgf20* may be functionally and evolutionarily significant, due to the tonotopic organization of the organ of Corti. The basal end of the organ of Corti detects high frequency sound, while the apical end detects low frequency sound (Basch et al., 2016). Therefore, disruptions to the cochlear base selectively causes high-frequency hearing loss. This further suggests that the decoupling of specification and differentiation, resulting in delayed differentiation of the cochlear apex, may offer a selective advantage in preferentially protecting low-frequency sound detection over high-frequency sound detection against genetic perturbations.

Here, we use cell cycle exit in the prosensory domain (also known as the zone of non-proliferation) as a marker for the completion of specification (P. Chen & Segil, 1999). Cell cycle exit itself does not need to occur prior to the onset of differentiation, as mice lacking $p27^{Kip1}$, which is required for cell cycle exit, still produce HCs and SCs (P. Chen & Segil, 1999; Kanzaki et al., 2006). Other proposed markers of the prosensory domain include $p27^{Kip1}$ and *Sox2*. However, since we disrupted *Sox2* expression, which leads to disruptions to $p27^{Kip1}$ expression (Kiernan et al., 2005), we determined that the best markers for full specification of the prosensory domain are cell cycle exit and nuclei shift away from the cochlear luminal surface.

Notably, while we show the potential for a *Sox2* and *Fgf20* interaction in modulating the temporal buffer between specification and differentiation, *Sox2* also has known roles during HC and SC differentiation (Ahmed et al., 2012; Dabdoub et al., 2008; Kempfle, Turban, & Edge, 2016; Puligilla & Kelley, 2016). Therefore, the genetic interaction may occur during differentiation as well. While interaction at this stage may explain the preferential loss of outer compartment cells in *Sox2* and *Fgf20* mutants, it does not explain the selective loss of basal cochlear HCs and SCs. Therefore, we conclude that the *Sox2* and *Fgf20* interaction regulates the temporal buffer, with potential further interactions during differentiation.

Outer compartment of the cochlear sensory epithelium is more sensitive to the loss of *Fgfr1, Fgf20*, and *Sox2* than the inner compartment.

In all of the genotypes we observed in this study, the loss of outer compartment cells (i.e. OHCs) was predominant. Only in the most severe cases in which almost all OHCs were missing, as seen in Fgfr1-CKO, $Fgf20^{-/-}$;$Sox2^{Ysb/Ysb}$, and $Sox2^{Ysb/-}$ cochleae, were IHCs also lost. Similarly, reduction in SC number always preferentially affected the outermost cells. This suggests that the organ of Corti outer compartment is more sensitive to the loss of *Fgfr1*, *Fgf20,* and *Sox2* than the inner compartment. The combination of $Fgf20^{-}$ and $Sox2^{Ysb}$ alleles elegantly demonstrates this: as the number of $Fgf20^{-}$ and $Sox2^{Ysb}$ alleles increased, the number of OHCs progressively decreased. In the double homozygous mutants, the number of IHCs decreased as well.

Previous studies noted that the dosage of *Fgfr1* affects the degree of organ of Corti outer compartment loss. In *Fgfr1* hypomorphs with 80% reduction in transcription, only the third row of OHCs were missing, while 90% hypomorphs had a slightly more severe phenotype (Pirvola et al., 2002). Therefore, *Fgfr1* loss preferentially affects the outermost HCs. Other studies

suggested that the timing of *Fgfr1* deletion affects *Sox2* expression decrease and the degree of outer compartment loss. When an earlier-expressed Cre driver (Six1enh21-Cre) was used to conditionally delete *Fgfr1*, almost all OHCs and some IHCs were lost, with a 66% reduction in *Sox2* expression at E14.5 (Ono et al., 2014). When a later-expressed Cre driver (*Emx2*^{Cre}) was used, many more OHCs and IHCs remained, with only a 12% reduction in *Sox2* expression. Our results are consistent with both of these studies. We show that FGF20-independent FGFR1 signaling and *Sox2* are required early, affecting both IHC and OHC development, while FGF20-FGFR1 signaling is important during later stages, affecting only OHC development.

Differentiation in the cochlea not only occurs in a basal-to-apical gradient, but also occurs in an orthogonal inner-to-outer gradient. That is, IHCs differentiate first, followed by each sequential row of OHCs (Ping Chen, Johnson, Zoghbi, & Segil, 2002). This wave of differentiation suggests that perhaps outer compartment HCs and SCs require a longer temporal buffer between specification and differentiation. The genetic interaction between *Sox2* and *Fgf20* in modulating this temporal buffer, therefore, could also account for the loss of outer compartment HCs and SCs. We hypothesize that the requirement for a longer temporal buffer may also be involved in determining OHC fate. In *Fgf20*$^{+/-}$;*Sox2*$^{+/-}$ cochleae, there was a slight decrease in OHCs that was compensated for by ectopic IHCs, suggesting a fate switch from OHCs into IHCs. Here, we confirmed previous suggestions that *Fgf20* regulates *Hey1* and *Hey2* to prevent premature differentiation in the developing organ of Corti (Benito-Gonzalez & Doetzlhofer, 2014; Tateya et al., 2013). Interestingly, in *Hey1*/*Hey2* double knockout cochleae, there was a similar slight decrease in OHCs compensated for by ectopic IHCs (Benito-Gonzalez & Doetzlhofer, 2014). Furthermore, inner ear-specific deletion of either *Smoothened* or *Neurod1*, which led to premature differentiation in the apical cochlear turn, also led to loss of OHCs and presence of ectopic IHCs at the apex (Jahan et al., 2010; Tateya et al., 2013). These findings further support a model where timing of specification and differentiation affect IHC versus OHC fate, an interesting and important topic for future studies.

Hey1/*Hey2* double knockout cochleae do not exhibit a loss of OHCs to the extent of Fgf20-KO cochleae, suggesting that other genes downstream of *Fgf20* are important in organ of Corti development. Interestingly, deletion of *N-Myc* and *L-Myc* from the cochlear epithelium results in accelerated cell cycle exit and delayed initiation of differentiation (Kopecky, Jahan, & Fritzsch, 2013), opposite to the effects of loss of *Sox2* and *Fgf20*. Addressing potential interactions between *Sox2*, *Fgf20*, *N-Myc*, and *L-Myc* is another topic for future studies.

Previously, we hypothesized that *Fgf20* is strictly required for the differentiation of an outer compartment progenitor (Huh et al., 2012). However, data we present here show that *Fgf20*, on a sensitized, *Sox2* hypomorphic background, is also required for inner compartment differentiation. We conclude that inner and outer compartment progenitors likely are not distinct populations. Rather, all prosensory progenitors giving rise to the organ of Corti exist on an inner-to-outer continuum. FGF20 signaling, in combination with other factors including Sox2, are required for the proper development of all of these cells, though with varying sensitivities.

MATERIALS AND METHODS

Mice

Mice were group housed with littermates, in breeding pairs, or in a breeding harem (2 females to 1 male), with food and water provided ad libitum.

For timed-pregnancy experiments, embryonic day 0.5 (E0.5) was assigned as noon of the day the vaginal plug was found. For postnatal experiments, postnatal day 0 (P0) was determined as the day of birth.

Mice were of mixed sexes and maintained on a mixed C57BL/6J x 129X1/SvJ genetic background. All mice were backcrossed at least three generations onto this background. The following mouse lines were used:

- *Fgf20*^{Cre} (*Fgf20*$^{-}$): knockin allele containing a sequence encoding a GFP-Cre fusion protein replacing exon 1 of *Fgf20*, resulting in a null mutation (Huh et al., 2015).
- *Fgf20*$^{\beta gal}$: knockin allele containing a sequence encoding β-galactosidase (βgal) replacing exon 1 of *Fgf20*, resulting in a null mutation (Huh et al., 2012).
- *Foxg1*^{Cre}: knockin allele containing a sequence encoding Cre fused in-frame downstream of the first 13 codons, resulting in a null mutation (Hébert & McConnell, 2000).
- *Fgfr1*^{flox}: allele containing loxP sequences flanking exons 8 through 15 of *Fgfr1*. Upon Cre-mediated recombination, produces a null mutation (Trokovic, Trokovic, Mai, & Partanen, 2003)
- *Fgfr1*$^{-}$: null allele generated by combining *Fgfr1*^{flox} with *Sox2*^{Cre} (S. Hayashi, Lewis, Pevny, & McMahon, 2002) to delete *Fgfr1* from the epiblast.
- *ROSA*^{rtTA}: knockin allele containing a loxP-Stop-loxP sequence followed by a sequence encoding rtTA-IRES-eGFP, targeted to the ubiquitously expressed *ROSA26* locus. Upon Cre-mediated recombination, reverse tetracycline transactivator (rtTA) and eGFP are expressed (Belteki et al., 2005).
- TRE-Fgf9-IRES-eGfp: transgene containing seven tetracycline-inducible regulatory elements driving the expression of FGF9-IRES-eGFP (White et al., 2006).
- *Sox2*^{Ysb}: Inner ear specific *Sox2* hypomorphic allele resulting from a random insertion of a transgene in chromosome 3, likely interfering with tissue-specific *Sox2* regulatory elements (Dong et al., 2002).
- *Sox2*$^{-}$: null allele generated by combining *Sox2*^{flox} (Shaham et al., 2009) with *Sox2*^{Cre} to delete *Sox2* from the epiblast.

All studies performed were in accordance with the Institutional Animal Care and Use Committee at Washington University in St. Louis and University of Nebraska Medical Center (protocol #16-004-02 and 16-005-02).

Doxycycline induction

Pregnant dams were starved overnight the night before initiation of Dox induction and fed Dox Diet, Grain-Based Doxycycline, 200 mg/kg (S3888, Bio-Serv, Flemington, NJ) ad libitum starting at noon on the start date of Dox induction. On the stop date of Dox induction, Dox Diet was replaced with regular mouse chow at noon.

Sample preparation and sectioning

For whole mount cochleae, inner ears were dissected out of P0 pups and fixed in 4% PFA in PBS overnight at 4°C with gentle agitation. Samples were then washed x3 in PBS. Cochleae were dissected away from the vestibule, otic capsule, and periotic mesenchyme with Dumont #55 Forceps (RS-5010, Roboz, Gaithersburg, MD). The roof of the cochlear duct was opened up by dissecting away the stria vascularis and Reissner's membrane; tectorial membrane was removed to expose hair and supporting cells.

For sectioning, heads from E14.5 embryos were fixed in 4% PFA in PBS overnight at 4°C with gentle agitation. Samples were then washed x3 in PBS and cryoprotected in 15% sucrose in PBS overnight and then in 30% sucrose in PBS overnight. Samples were embedded in Tissue-Tek O.C.T. compound (4583, VWR International, Radnor, PA) and frozen on dry ice. Serial horizontal sections through base of the head were cut at 12 µm with a cryostat, dried at room temperature, and stored at -80°C until use.

RNA in situ hybridization

Probe preparation: mouse cDNA plasmids containing the following inserts were used to make RNA in situ probes, and were cut and transcribed with the indicated restriction enzyme (New England Biolabs, Ipswich, MA) and RNA polymerase (New England Biolabs, Ipswich, MA): *Fgfr1* transmembrane domain (325 bp, HincII, T7, gift of K Peters), *Fgf20* (653 bp, NcoI, Sp6), *Sox2* (750 bp, AccI, T3, gift of R. Lovell-Badge), *Etv4* (~2300 bp, ApaI, Sp6, gift of G. Martin), *Etv5* (~4000 bp, HindIII, T3, gift of G. Martin), *Hey1* (343 bp, EcoRI, T3, gift of S. Rentschler), *Hey2* (819 bp, EcoRI, T7, gift of S. Rentschler). Restriction digest and *in vitro* transcription were done according to manufacturer's instructions, with DIG RNA Labeling Mix (11277073910, Sigma-Aldrich, St. Louis, MO). After treatment with RNase-free DNase I (04716728001, Sigma-Aldrich, St. Louis, MO) for 15 min at 37°C, probes were hydrolyzed in hydrolysis buffer (40 mM $NaHCO_3$, 60 mM Na_2CO_3) at 60°C for up to 30 min, depending on probe size.

Frozen section in situ hybridization: frozen slides were warmed for 20 min at room temperature and then 5 min at 50°C on a slide warmer. Sections were fixed in 4% PFA in PBS for 20 min at room temperature, washed x2 in PBS and treated with pre-warmed 10 µg/ml Proteinase K (03115828001, Sigma-Aldrich, St. Louis, MO) in PBS for 7 min at 37°C. Sections were then fixed in 4% PFA in PBS for 15 min at room temperature, washed x2 in PBS, acetylated in 0.25% acetic anhydrate in 0.1M Triethanolamine, pH 8.0, for 10 min, and washed again in PBS. Sections were then placed in pre-warmed hybridization buffer (50% formamide, 5x SSC buffer, 5 mM EDTA, 50 µg/ml yeast tRNA) for 3 h at 60°C in humidified chamber for prehybridization. Sections were then hybridized in 10 µg/ml probe/hybridization buffer overnight (12-16 h) at 60°C. The next day, sections were washed in 1x SSC for 10 min at 60°C, followed by 1.5x SSC for 10 min at 60°C, 2x SSC for 20 min at 37°C x2, and 0.2x SSC for 30 min at 60°C x2. Sections were then washed in KTBT (0.1 M Tris, pH 7.5, 0.15 M NaCl, 5 mM KCl, 0.1% Triton X-100) at room temperature and blocked in KTBT + 20% sheep serum + 2% Blocking Reagent (11096176001, Sigma-Aldrich, St. Louis, MO) for 4 h. Blocking Reagent was dissolved in 100 mM Maleic acid, 150 mM NaCl, pH 7.5. Sections were then incubated in sheep anti-Digoxigenin-AP, Fab fragments (1:1000, 11093274910, Sigma-Aldrich, St. Louis, MO) in KTBT + 20% sheep serum + 2% Blocking Reagent overnight at 4°C. Sections were then washed x3 in KTBT for 30 min at room temperature, and then washed x2 in NTMT (0.1 M Tris, pH 9.5, 0.1 M NaCl, 50 mM $MgCl_2$, 0.1% Tween 20) for 15 min. Sections were next incubated in NTMT + 1:200 NBT/BCIP Stock Solution (11681451001, Sigma-Aldrich, St. Louis, MO) in the dark at room temperature until color appeared. Sections were then washed in PBS, post-fixed in 4% PFA in PBS for 15 min and washed x2 in PBS. Finally, sections were dehydrated in 30% and then 70% methanol, 5 min each, followed by 100% methanol for 15 min. Sections were then rehydrated in 70% and 30% methanol and then PBS, 5 min each, and mounted in 95% glycerol.

Immunofluorescence

Whole mount: cochleae were incubated in PBS + 0.5% Tween-20 (PBSTw) for 1 h to permeabilize. Cochleae were then blocked using PBSTw + 5% donkey serum for 1 h and then incubated in PBSTw + 1% donkey serum with the primary antibody overnight at 4°C. Cochleae were then washed x3 in PBS and incubated in PBS + 1% Tween-20 with the secondary antibody. After wash in PBS x3, cochleae were mounted in 95% glycerol with the sensory epithelium facing up.

Frozen slides were warmed for 30 min at room temperature and washed in PBS before incubating in PBS + 0.5% Triton X-100 (PBST) for 1 h to permeabilize the tissue. Sections were then blocked using in PBST + 5% donkey serum for 1 h and then incubated in PBST + 1% donkey serum with the primary antibody overnight at 4°C in a humidified chamber. Sections were then washed x3 in PBS and incubated in PBS + 1% Triton X-100 with the secondary antibody. After wash in PBS x3, slides were mounted in VectaShield antifade mounting medium with DAPI (H-1200, Vector Labs, Burlingame, CA).

The following compounds and antibodies were used:

- Alexa Fluor 488-conjugated Phallodin (1:50, A12379, Invitrogen, Carlsbad, CA)
- Rabbit anti-p75NTR (1:300, AB1554, EMD Millipore, Burlington, MA)
- Rabbit anti-Prox1 (1:1000, ABN278, EMD Millipore, Burlington, MA)
- Goat anti-Sox2 (1:200, sc-17320, Santa Cruz Biotechnology, Dallas, TX)
- Rabbit anti-Ki67 (1:200, ab15580, Abcam, Cambridge, United Kingdom)
- Rabbit anti-Myo6 (1:100, sc-50461, Santa Cruz Biotechnology, Dallas, TX)
- Alexa Fluor conjugated secondary antibodies (1:500; Thermo-Fisher Scientific, Waltham, MA)
- Sheep anti-Digoxigenin-AP, Fab fragments (1:1000, 11093274910, Sigma-Aldrich, St. Louis, MO)

Cell proliferation assay

EdU (E10187, Thermo-Fisher Scientific, Waltham, MA) was injected i.p. into pregnant dams at 100 µg per gram body weight. Embryos were harvested at 1 h after injection. EdU was detected using the Click-iT EdU Alexa Fluor 488 kit (C10337, Thermo-Fisher Scientific, Waltham, MA) according to manufacturer's instructions.

Imaging

Brightfield microscopy was done using a Hamamatsu NanoZoomer slide scanning system with a 20x objective. Images were processed with the NanoZoomer Digital Pathology (NDP.view2) software.

Fluorescent microscopy was done using a Zeiss LSM 700 confocal or Zeiss Axio Imager Z1 with Apotome 2, with z-stack step-size determined based on objective lens type (10x or 20x), as recommended by the ZEN software (around 1 µm). Fluorescent images shown are maximum projections. Low magnification fluorescent images shown of the whole cochlear duct required stitching together, by hand, several images. Images were processed with ImageJ (imagej.nih.gov).

Quantification

Measurements and cell quantification (using the Cell Counter plugin by Kurt De Vos) were done using ImageJ. Total cochlear duct length was defined as the length from the very base of the cochlea to the very tip of the apex, along the tunnel of Corti. Hair cells were identified via Phalloidin, which binds to F-actin (Avinash, Nuttall, & Raphael, 1993). Inner pillar cells were labeled via p75NTR (Mueller, Jacques, & Kelley, 2002), and supporting cells (SCs, including pillar cells and Deiters' cells) were labeled with a combination of Prox1 (Bermingham-McDonogh et al., 2006) and Sox2 (Mak et al., 2009). Inner hair cells (IHCs) were differentiated from outer hair cells (OHCs) based on their neural/abneural location, respectively, relative to p75NTR-expressing inner pillar cells. For total cell counts, IHCs, OHCs, and SCs were counted along the entire length of the cochlea. Total cell counts were also normalized to cochlear length and presented as cell count per 100 µm of cochlea (e.g. IHCs/100 µm). For cell quantification at the basal, middle, and apical turns of the cochlea, the cochlear duct was evenly divided into thirds, and total IHCs, OHCs, and SCs were quantified for each third and normalized to length. For the Fgf20-rescue experiments in Figure 3, IHCs, OHCs, and SCs from at least 300 µm regions of the basal (10%), middle (40%), and apical (70%) turns of the cochleae were counted and normalized to 100 µm along the length of the cochlear duct.

In $Sox2^{Ysb/-}$ cochleae, p75NTR expression was mostly absent, resulting in sensory islands without p75NTR-expressing inner pillar cells. In these cochleae, HCs not associated with inner pillar cells were presumed to be IHCs during quantification. When a curved line was drawn connecting the p75NTR islands along the organ of Corti, these presumed IHCs were always medial (neural) to that line.

Statistical analysis and plotting

All figures were made in Canvas X (ACD systems). Data analysis was performed using the Python programming language (python.org) in Jupyter Notebook (jupyter.org) with the following libraries: Pandas (pandas.pydata.org), NumPy (numpy.org) and SciPy (scipy.org). Plotting was done using the Matplotlib library (matplotlib.org). Statistics (t-test, one-way ANOVA, and two-way ANOVA) were performed using the SciPy module Stats; Tukey's HSD was performed using the Statsmodels package (statsmodels.org). All comparisons of two means were performed using two-tailed, unpaired Student's t-test. For comparisons of more than two means, one-way ANOVA was used, except in Figures 7 and supplement 1, where two-way ANOVA was used, with the factors being *Fgf20* (levels: $Fgf20^{+/+}$, $Fgf20^{+/-}$, $Fgf20^{-/-}$) and *Sox2* (levels: $Sox2^{+/+}$, $Sox2^{Ysb/+}$, $Sox2^{Ysb/Ysb}$) gene dosage. For significant ANOVA results at $\alpha = 0.05$, Tukey's HSD was performed for post-hoc pair-wise analysis. In all cases, $p < 0.05$ was considered statistically significant. All statistical details can be found in the figures and figure legends. In all cases, each sample represents one animal. Data are represented as mean ± standard deviation. For qualitative comparisons (comparing expression via immunofluorescence or RNA in situ hybridization), at least three samples were examined per genotype. All images shown are representative.

ACKNOWLEDGEMENTS

This work was funded by the March of Dimes Foundation, the Department of Developmental Biology at Washington University, DC017042 (DMO), DC012825 (S.H.), GM110768 (S.H.), HOPE Center Alafi Neuroimaging Laboratory (NCRR 1S10RR027552), and the Auditory and Vestibular Microscopy and Digital Imaging Core (NIH P30 DC004665).

AUTHOR CONTRIBUTIONS

Conceptualization, L.M.Y., S.H., and D.M.O.; Methodology, L.M.Y., S.H., and D.M.O.; Formal Analysis, L.M.Y. and S.H.; Investigation: L.M.Y. and S.H.; Resources: D.M.O.; Writing – Original Draft: L.M.Y. and D.M.O.; Writing – Review & Editing: L.M.Y., S.H., and D.M.O.; Supervision: D.M.O.; Funding Acquisition: S.H. and D.M.O.

COMPETING INTERESTS

The authors declare no competing interests.

REFERENCES

Ahmed, M., Wong, E. Y. M., Sun, J., Xu, J., Wang, F., & Xu, P.-X. (2012). Eya1-Six1 Interaction Is Sufficient to Induce Hair Cell Fate in the Cochlea by Activating Atoh1 Expression in Cooperation with Sox2. *Developmental Cell*, *22*(2), 377–390. https://doi.org/10.1016/j.devcel.2011.12.006

Avinash, G. B., Nuttall, A. L., & Raphael, Y. (1993). 3-D analysis of F-actin in stereocilia of cochlear hair cells after loud noise exposure. *Hearing Research*, *67*(1), 139–146. https://doi.org/10.1016/0378-5955(93)90241-R

Basch, M. L., Brown, R. M., Jen, H.-I., & Groves, A. K. (2016). Where hearing starts: the development of the mammalian cochlea. *Journal of Anatomy*, *228*(2), 233–254. https://doi.org/10.1111/joa.12314

Belteki, G., Haigh, J., Kabacs, N., Haigh, K., Sison, K., Costantini, F., … Nagy, A. (2005). Conditional and inducible transgene expression in mice through the combinatorial use of Cre-mediated recombination and tetracycline induction. *Nucleic Acids Research*, *33*(5), e51–e51. https://doi.org/10.1093/nar/gni051

Benito-Gonzalez, A., & Doetzlhofer, A. (2014). Hey1 and Hey2 Control the Spatial and Temporal Pattern of Mammalian Auditory Hair Cell Differentiation Downstream of Hedgehog Signaling. *Journal of Neuroscience*, *34*(38), 12865–12876. https://doi.org/10.1523/JNEUROSCI.1494-14.2014

Bermingham-McDonogh, O., Oesterle, E. C., Stone, J. S., Hume, C. R., Huynh, H. M., & Hayashi, T. (2006). Expression of Prox1 during mouse cochlear development. *Journal of Comparative Neurology*, *496*(2), 172–186. https://doi.org/10.1002/cne.20944

Bok, J., Zenczak, C., Hwang, C. H., & Wu, D. K. (2013). Auditory ganglion source of Sonic hedgehog regulates timing of cell cycle exit and differentiation of mammalian cochlear hair cells. *Proceedings of the National Academy of Sciences of the United States of America*, *110*(34), 13869–13874. https://doi.org/10.1073/pnas.1222341110

Brown, A. S., & Epstein, D. J. (2011). Otic ablation of smoothened reveals direct and indirect requirements for Hedgehog signaling in inner ear development. *Development*, *138*(18), 3967–3976. https://doi.org/10.1242/dev.066126

Chen, P., & Segil, N. (1999). p27(Kip1) links cell proliferation to morphogenesis in the developing organ of Corti. *Development*, *126*(8), 1581–1590.

Chen, Ping, Johnson, J. E., Zoghbi, H. Y., & Segil, N. (2002). The role of Math1 in inner ear development: Uncoupling the establishment of the sensory primordium from hair cell fate determination. *Development*, *129*(10), 2495–2505.

Dabdoub, A., Puligilla, C., Jones, J. M., Fritzsch, B., Cheah, K. S. E., Pevny, L. H., & Kelley, M. W. (2008). Sox2 signaling in prosensory domain specification and subsequent hair cell differentiation in the developing cochlea. *Proceedings of the National Academy of*

Sciences of the United States of America, *105*(47), 18396–18401. https://doi.org/10.1073/pnas.0808175105

Dong, S., Leung, K. K. H., Pelling, A. L., Lee, P. Y. T., Tang, A. S. P., Heng, H. H. Q., … Steel, K. P. (2002). Circling, Deafness, and Yellow Coat Displayed by Yellow Submarine (Ysb) and Light Coat and Circling (Lcc) Mice with Mutations on Chromosome 3. *Genomics*, *79*(6), 777–784. https://doi.org/10.1006/geno.2002.6783

Ebeid, M., & Huh, S.-H. (2017). FGF signaling: diverse roles during cochlear development. *BMB Reports*, *50*(10), 487–495. https://doi.org/10.5483/BMBRep.2017.50.10.164

Fekete, D. M., Muthukumar, S., & Karagogeos, D. (1998). Hair Cells and Supporting Cells Share a Common Progenitor in the Avian Inner Ear. *Journal of Neuroscience*, *18*(19), 7811–7821. https://doi.org/10.1523/JNEUROSCI.18-19-07811.1998

Gu, R., Brown, R. M., Hsu, C.-W., Cai, T., Crowder, A. L., Piazza, V. G., … Groves, A. K. (2016). Lineage tracing of Sox2-expressing progenitor cells in the mouse inner ear reveals a broad contribution to non-sensory tissues and insights into the origin of the organ of Corti. *Developmental Biology*, *414*(1), 72–84. https://doi.org/10.1016/j.ydbio.2016.03.027

Hayashi, S., Lewis, P., Pevny, L., & McMahon, A. P. (2002). Efficient gene modulation in mouse epiblast using a Sox2Cre transgenic mouse strain. *Mechanisms of Development*, *119 Suppl 1*, S97–S101.

Hayashi, T., Ray, C. A., & Bermingham-McDonogh, O. (2008). Fgf20 Is Required for Sensory Epithelial Specification in the Developing Cochlea. *Journal of Neuroscience*, *28*(23), 5991–5999. https://doi.org/10.1523/JNEUROSCI.1690-08.2008

Hébert, J. M., & McConnell, S. K. (2000). Targeting of cre to the Foxg1 (BF-1) Locus Mediates loxP Recombination in the Telencephalon and Other Developing Head Structures. *Developmental Biology*, *222*(2), 296–306. https://doi.org/10.1006/dbio.2000.9732

Huh, S.-H., Jones, J., Warchol, M. E., & Ornitz, D. M. (2012). Differentiation of the Lateral Compartment of the Cochlea Requires a Temporally Restricted FGF20 Signal. *PLOS Biology*, *10*(1), e1001231. https://doi.org/10.1371/journal.pbio.1001231

Huh, S.-H., Warchol, M. E., & Ornitz, D. M. (2015). Cochlear progenitor number is controlled through mesenchymal FGF receptor signaling. *ELife*, *4*, e05921. https://doi.org/10.7554/eLife.05921

Jahan, I., Pan, N., Kersigo, J., & Fritzsch, B. (2010). Neurod1 Suppresses Hair Cell Differentiation in Ear Ganglia and Regulates Hair Cell Subtype Development in the Cochlea. *PLOS ONE*, *5*(7), e11661. https://doi.org/10.1371/journal.pone.0011661

Kanzaki, S., Beyer, L. A., Swiderski, D. L., Izumikawa, M., Stöver, T., Kawamoto, K., & Raphael, Y. (2006). p27Kip1 deficiency causes organ of Corti pathology and hearing loss. *Hearing Research*, *214*(1), 28–36. https://doi.org/10.1016/j.heares.2006.01.014

Kelley, M. W. (2007). Cellular commitment and differentiation in the organ of Corti. *The International Journal of Developmental Biology*, *51*(6–7), 571–583. https://doi.org/10.1387/ijdb.072388mk

Kempfle, J. S., Turban, J. L., & Edge, A. S. B. (2016). Sox2 in the differentiation of cochlear progenitor cells. *Scientific Reports*, *6*, 23293. https://doi.org/10.1038/srep23293

Kiernan, A. E., Pelling, A. L., Leung, K. K. H., Tang, A. S. P., Bell, D. M., Tease, C., … Cheah, K. S. E. (2005). Sox2 is required for sensory organ development in the mammalian inner ear. *Nature*, *434*(7036), 1031–1035. https://doi.org/10.1038/nature03487

Kopecky, B. J., Jahan, I., & Fritzsch, B. (2013). Correct Timing of Proliferation and Differentiation is Necessary for Normal Inner Ear Development and Auditory Hair Cell Viability: Mycs' Role in Ear Development. *Developmental Dynamics*, *242*(2), 132–147. https://doi.org/10.1002/dvdy.23910

Lee, Y.-S., Liu, F., & Segil, N. (2006). A morphogenetic wave of p27Kip1 transcription directs cell cycle exit during organ of Corti development. *Development*, *133*(15), 2817–2826. https://doi.org/10.1242/dev.02453

Mak, A. C. Y., Szeto, I. Y. Y., Fritzsch, B., & Cheah, K. S. E. (2009). Differential and overlapping expression pattern of SOX2 and SOX9 in inner ear development. *Gene Expression Patterns*, *9*(6), 444–453. https://doi.org/10.1016/j.gep.2009.04.003

Matei, V., Pauley, S., Kaing, S., Rowitch, D., Beisel, K. w., Morris, K., … Fritzsch, B. (2005). Smaller inner ear sensory epithelia in Neurog1 null mice are related to earlier hair cell cycle exit. *Developmental Dynamics*, *234*(3), 633–650. https://doi.org/10.1002/dvdy.20551

Mueller, K. L., Jacques, B. E., & Kelley, M. W. (2002). Fibroblast Growth Factor Signaling Regulates Pillar Cell Development in the Organ of Corti. *Journal of Neuroscience*, *22*(21), 9368–9377.

Munnamalai, V., Hayashi, T., & Bermingham-McDonogh, O. (2012). Notch Prosensory Effects in the Mammalian Cochlea Are Partially Mediated by Fgf20. *Journal of Neuroscience*, *32*(37), 12876–12884. https://doi.org/10.1523/JNEUROSCI.2250-12.2012

Ono, K., Kita, T., Sato, S., O'Neill, P., Mak, S.-S., Paschaki, M., … Ladher, R. K. (2014). FGFR1-Frs2/3 Signalling Maintains Sensory Progenitors during Inner Ear Hair Cell Formation. *PLOS Genetics*, *10*(1), e1004118. https://doi.org/10.1371/journal.pgen.1004118

Ornitz, D. M., & Itoh, N. (2015). The Fibroblast Growth Factor signaling pathway. *Wiley Interdisciplinary Reviews: Developmental Biology*, *4*(3), 215–266. https://doi.org/10.1002/wdev.176

Pan, W., Jin, Y., Chen, J., Rottier, R. J., Steel, K. P., & Kiernan, A. E. (2013). Ectopic Expression of Activated Notch or SOX2 Reveals Similar and Unique Roles in the Development of the Sensory Cell Progenitors in the Mammalian Inner Ear. *Journal of Neuroscience*, *33*(41), 16146–16157. https://doi.org/10.1523/JNEUROSCI.3150-12.2013

Pauley, S., Lai, E., & Fritzsch, B. (2006). Foxg1 is required for morphogenesis and histogenesis of the mammalian inner ear. *Developmental Dynamics*, *235*(9), 2470–2482. https://doi.org/10.1002/dvdy.20839

Pirvola, U., Ylikoski, J., Trokovic, R., Hébert, J. M., McConnell, S. K., & Partanen, J. (2002). FGFR1 is required for the development of the auditory sensory epithelium. *Neuron*, *35*(4), 671–680.

Puligilla, C., & Kelley, M. W. (2016). Dual role for Sox2 in specification of sensory competence and regulation of Atoh1 function. *Developmental Neurobiology*, *77*(1), 3–13. https://doi.org/10.1002/dneu.22401

Scholzen, T., & Gerdes, J. (2000). The Ki-67 protein: From the known and the unknown. *Journal of Cellular Physiology*, *182*(3), 311–322. https://doi.org/10.1002/(SICI)1097-4652(200003)182:3<311::AID-JCP1>3.0.CO;2-9

Shaham, O., Smith, A. N., Robinson, M. L., Taketo, M. M., Lang, R. A., & Ashery-Padan, R. (2009). Pax6 is essential for lens fiber cell differentiation. *Development*, *136*(15), 2567–2578. https://doi.org/10.1242/dev.032888

Tateya, T., Imayoshi, I., Tateya, I., Hamaguchi, K., Torii, H., Ito, J., & Kageyama, R. (2013). Hedgehog signaling regulates prosensory cell properties during the basal-to-apical wave of hair cell differentiation in the mammalian cochlea. *Development*, *140*(18), 3848–3857. https://doi.org/10.1242/dev.095398

Trokovic, N., Trokovic, R., Mai, P., & Partanen, J. (2003). Fgfr1 regulates patterning of the pharyngeal region. *Genes & Development*, *17*(1), 141–153. https://doi.org/10.1101/gad.250703

White, A. C., Xu, J., Yin, Y., Smith, C., Schmid, G., & Ornitz, D. M. (2006). FGF9 and SHH signaling coordinate lung growth and development through regulation of distinct

mesenchymal domains. *Development*, *133*(8), 1507–1517. https://doi.org/10.1242/dev.02313

Zhang, X., Ibrahimi, O. A., Olsen, S. K., Umemori, H., Mohammadi, M., & Ornitz, D. M. (2006). Receptor Specificity of the Fibroblast Growth Factor Family: THE COMPLETE MAMMALIAN FGF FAMILY. *Journal of Biological Chemistry*, *281*(23), 15694–15700. https://doi.org/10.1074/jbc.M601252200

FIGURE TITLES AND LEGENDS

Figure 1. The Fgf20-KO cochlear phenotype is less severe than the Fgfr1-CKO phenotype

(A, B) Whole mount cochlea from P0 *Fgf20*$^{+/-}$, *Fgf20*$^{-/-}$, *Foxg1*$^{Cre/+}$;*Fgfr1*$^{flox/+}$, and *Foxg1*$^{Cre/+}$;*Fgfr1*$^{flox/-}$ mice showing (A) inner and outer hair cells (IHC and OHC, phalloidin, green) separated by inner pillar cells (p75NTR, red) and (B) supporting cells (Prox1 and Sox2, green/yellow). Magnifications show the basal, middle, and apical turns of the cochlea. Scale bar, 100 µm (magnifications), 1 mm (whole).

(C-F) Quantification of (C) cochlear duct length, (D) total IHCs and IHCs per 100 µm of the cochlear duct, (E) total OHCs and OHCs per 100 µm, and (F) total supporting cells (SCs) and SCs per 100 µm at P0. *Fgf20*$^{+/-}$ and *Fgf20*$^{-/-}$ cochleae results were analyzed by unpaired Student's t test; *Fgfr1*$^{flox/+}$, *Fgfr1*$^{flox/-}$, *Foxg1*$^{Cre/+}$;*Fgfr1*$^{flox/+}$, and *Foxg1*$^{Cre/+}$;*Fgfr1*$^{flox/-}$ cochleae results were analyzed by one-way ANOVA. P values shown are from the t test and ANOVA. * indicates $p < 0.05$ from Student's t test or Tukey's HSD (ANOVA post-hoc); n.s., not significant.

(G) A model of organ of Corti development, which occurs in two steps: prosensory specification and differentiation. It is not definitively known which step FGFR1 signaling, with FGF20 and unidentified ligand(s), has a role in.

See also Figure 1—Figure supplement 1.

Figure 2. FGFR1 regulates Sox2 expression while FGF20 does not

(A) Sections through the middle turn of E14.5 cochlear ducts from *Fgf20*$^{+/-}$, *Fgf20*$^{-/-}$, *Foxg1*$^{Cre/+}$;*Fgfr1*$^{flox/+}$, and *Foxg1*$^{Cre/+}$;*Fgfr1*$^{flox/-}$ mice. RNA in situ hybridization (top) and immunofluorescence for *Sox2* (red, bottom), which is expressed in the prosensory domain at this stage. Refer to schematic in (B). DAPI, nuclei (blue). Scale bar, 100 µm.

(B) Schematic of a cross section through the middle turn of the E14.5 cochlear duct. The floor of the cochlear duct is categorized into three zones: outer sulcus (OS), prosensory domain (PD), and Kölliker's organ (KO). Neural indicates the side of the duct towards the spiral ganglion cells; abneural indicates away.

(C) An updated model of organ of Corti development. Ligand X/FGFR1 signaling regulates *Sox2* expression during prosensory specification; FGF20/FGFR1 signaling regulates differentiation.

See also Figure 2—Figure supplement 1.

Figure 3. Genetic rescue of the Fgf20-KO phenotype suggests that FGF20 is required for differentiation

(A, B) Whole mount cochlea from P0 *Fgf20*$^{+/-}$;*ROSA*^{rtTA} (Fgf20-het), *Fgf20*$^{+/-}$;*ROSA*^{rtTA}; TRE-Fgf9-IRES-eGfp (Fgf9-OA), *Fgf20*$^{-/-}$;*ROSA*^{rtTA} (Fgf20-null), and *Fgf20*$^{-/-}$;*ROSA*^{rtTA}; TRE-Fgf9-IRES-eGfp (Fgf20-rescue) mice showing (A) inner and outer hair cells (phalloidin, green) separated by inner pillar cells (p75NTR, red) and (B) supporting cells (Prox1 and Sox2, green/yellow). Images from basal, middle, and apical turns of the cochlea are shown. Fgf20-rescue cochleae from four different doxycycline chow (Dox) regimens are shown (E13.5-E15.5, E13.5, E14.5, and E15.5). Fgf20-het, Fgf9-OA, and Fgf20-null cochleae shown are from the E13.5-E15.5 Dox regimen. Scale bar, 100 µm.

(C) Quantification of outer hair cells (OHC) and supporting cells (SC) from P0 Fgf9-OA (Dox regimen: E13.5-E15.5), Fgf20-null (Dox regimen: E13.5-E15.5), and Fgf20-rescue (all four Dox regimens) cochleae, presented as a percentage of the number of cells in Fgf20-het cochleae from the same Dox regimen. * indicates $p < 0.05$ compared to Fgf20-null cochleae from the same Dox regimen; ^ indicates $p < 0.05$ compared to

Fgf20-het cochleae from the same Dox regimen; Tukey's HSD (one-way ANOVA post-hoc).

See also Figure 3—Figure supplement 1.

Figure 4. Decrease in Sox2 expression results in similar phenotypes as disruptions to FGFR1 signaling

(A, B) Whole mount cochlea from P0 *Sox2*$^{+/+}$, *Sox2*$^{Ysb/+}$, *Sox2*$^{Ysb/Ysb}$, and *Sox2*$^{Ysb/-}$ mice showing (A) inner and outer hair cells (phalloidin, green) separated by inner pillar cells (p75NTR, red) and (B) supporting cells (Prox1 and Sox2, green/yellow). Magnifications show the basal, middle, and apical turns of the cochlea. Arrowheads indicate ectopic inner hair cells. Scale bar, 100 µm (magnifications), 1 mm (whole)

(C-F) Quantification of (C) cochlear duct length, (D) total inner hair cells (IHCs) and IHCs per 100 µm of the cochlear duct, (E) total outer hair cells (OHCs) and OHCs per 100 µm, and (F) total supporting cells (SCs) and SCs per 100 µm at P0. P values shown are from one-way ANOVA. * indicates $p < 0.05$ from Tukey's HSD (ANOVA post-hoc).

See also Figure 4—Figure supplement 1.

Figure 5. Decrease in levels of Sox2 expression delays prosensory specification

(A) Serial sections (1-6) through the duct of E14.5 and E15.5 *Sox2*$^{Ysb/+}$ and *Sox2*$^{Ysb/-}$ cochleae. Immunoflurescence for Ki67 (red) and DAPI (nuclei, cyan). Cochlear epithelium is outlined. Bracket indicates prosensory domain. * indicates shift of prosensory nuclei away from the luminal surface of the epithelium. N, neural side. Scale bar, 100 µm. See whole mount cochlear duct schematic (lower right) for relative positions of the serial sections.

(B) A model of organ of Corti development showing embryonic staging (x-axis) and location along the cochlear duct (basal, middle, and apical turns, y-axis). Development occurs in two stages: unspecified progenitors (tan shading) undergo specification and cell cycle exit to become prosensory cells (green shading), which then differentiate into hair cells and supporting cells (HCs & SCs; red shading). In wildtype cochleae, cell cycle exit (indicating completion of specification) begins at the apex of the cochlea and proceeds basally. Afterwards, differentiation initiates at the mid-base of the cochlea and proceeds basally and apically. Temporal buffer (green shading), which is narrow at the basal end of the cochlea but wide at the apical end, refers to the time between cell cycle exit and initiation of differentiation. In *Sox2* hypomorph cochleae, specification and cell cycle exit are delayed, resulting in failure to complete specification before initiation of differentiation towards the basal end of the cochlea (crosshatch pattern).

See also Figure 5—Figure supplement 1.

Figure 6. *Sox2 is upstream of Fgf20*

(A-C) Sections through the middle turn of E14.5 cochleae.

(A) RNA in situ hybridization for *Etv4* and *Etv5* in *Sox2*$^{Ysb/+}$ and *Sox2*$^{Ysb/-}$ cochleae. The two brackets indicate *Etv4/5* expression in the outer sulcus (OS, left) and prosensory domain (PD, right). Refer to schematic at the bottom.

(B) RNA in situ hybridization for *Fgfr1* and *Fgf20* in *Sox2*$^{Ysb/+}$ and *Sox2*$^{Ysb/-}$ cochleae. Bracket indicates *Fgfr1*/*Fgf20* expression in the prosensory domain.

(C) RNA in situ hybridization for *Fgf20* in *Foxg1*$^{Cre/+}$;*Fgfr1*$^{flox/+}$ and *Foxg1*$^{Cre/+}$;*Fgfr1*$^{flox/-}$ cochleae. Bracket indicates *Fgf20* expression in the prosensory domain.

(D) Serial sections (1-6) through the duct of E14.5 *Fgf20*$^{+/-}$ and *Fgf20*$^{-/-}$ cochleae. Immunoflurescence for Ki67 (red) and DAPI (nuclei, cyan). Cochlear epithelium is

outlined. Bracket indicates prosensory domain. * indicates shift of prosensory nuclei away from the luminal surface of the epithelium. N, neural side. Scale bar, 100 µm. See whole mount cochlear duct schematic (lower right) for relative positions of the serial sections.

(E) An updated model of organ of Corti development showing that *Sox2* acts upstream of *Fgf20*.

OS, outer sulcus; PD, prosensory domain; KO, Kölliker's organ. Scale bar, 100 µm. See also Figure 6—Figure supplement 1.

Figure 7. *Sox2* and *Fgf20* interact during cochlea development

(A, B) Whole mount cochlea from P0 *Fgf20*$^{+/-}$;*Sox2*$^{Ysb/+}$, *Fgf20*$^{+/-}$;*Sox2*$^{Ysb/Ysb}$, *Fgf20*$^{-/-}$;*Sox2*$^{Ysb/+}$, *Fgf20*$^{-/-}$;*Sox2*$^{Ysb/Ysb}$ mice showing (A) inner and outer hair cells (phalloidin, green) separated by inner pillar cells (p75NTR, red) and (B) supporting cells (Prox1 and Sox2, green/yellow). Magnifications show the basal, middle, and apical turns of the cochlea. Arrowheads indicate ectopic inner hair cells. Scale bar, 100 µm (magnifications), 1 mm (whole).

(C) P values from two-way ANOVA analyzing the quantification results in (D-G). The two factors analyzed are *Fgf20* (*Fgf20*$^{+/+}$, *Fgf20*$^{+/-}$, *Fgf20*$^{-/-}$) and *Sox2* (*Sox2*$^{+/+}$, *Sox2*$^{Ysb/+}$, *Sox2*$^{Ysb/Ysb}$) gene dosage. A p value < 0.05 (yellow highlight) for *Fgf20* or *Sox2* indicates that the particular factor (independent variable) has a statistically significant effect on the measurement (dependent variable). Whereas a p value < 0.05 for Interaction indicates a statistically significant interaction between the effects of the two factors on the measurement.

(D-G) Quantification of (D) cochlear duct length, (E) total inner hair cells (IHCs) and IHCs per 100 µm of the cochlear duct, (F) total outer hair cells (OHCs) and OHCs per 100 µm, and (G) total supporting cells (SCs) and SCs per 100 µm at P0 in *Fgf20*$^{+/+}$;*Sox2*$^{+/+}$, *Fgf20*$^{+/+}$;*Sox2*$^{Ysb/+}$, *Fgf20*$^{+/-}$;*Sox2*$^{+/+}$, *Fgf20*$^{+/-}$;*Sox2*$^{Ysb/+}$, *Fgf20*$^{+/+}$;*Sox2*$^{Ysb/Ysb}$, *Fgf20*$^{+/-}$;*Sox2*$^{Ysb/Ysb}$, *Fgf20*$^{-/-}$;*Sox2*$^{+/+}$, *Fgf20*$^{-/-}$;*Sox2*$^{Ysb/+}$, and *Fgf20*$^{-/-}$;*Sox2*$^{Ysb/Ysb}$ cochleae.

(H) Results from post-hoc Tukey's HSD analyzing the quantification results in (D-G). Letters (L, I, J, O, P, S, T; representing each measurement in panels D-G) indicate a statistically significant decrease (p < 0.05) when comparing the row genotype against the column genotype. L, cochlear length; I, total IHCs; J, IHCs/100 µm; O, total OHCs; P, OHCs/100 µm; S, total SCs; T, SCs/100 µm.

See also Figure 7—Figure supplements 1 and 2.

Figure 8. Fgf20-KO organ of Corti exhibits premature differentiation

(A) The *Fgf20*$^{-/-}$, *Foxg1*$^{Cre/+}$;*Fgfr1*$^{flox/-}$, *Fgf20*$^{-/-}$;*Sox2*$^{Ysb/Ysb}$, *Sox2*$^{Ysb/-}$ cochleae phenotypes lie along a continuum, preferentially affecting outer and basal cochlear sensory epithelium, likely attributable to varying *Sox2* levels on an *Fgf20*-null background.

(B) Serial sections (1-6) through the duct of E14.5 *Fgf20*$^{+/-}$;*Sox2*$^{Ysb/+}$, *Fgf20*$^{+/-}$;*Sox2*$^{Ysb/Ysb}$, *Fgf20*$^{-/-}$;*Sox2*$^{Ysb/+}$, *Fgf20*$^{-/-}$;*Sox2*$^{Ysb/Ysb}$ cochleae. Immunoflurescence for Ki67 (red) and DAPI (nuclei, cyan). Cochlear epithelium is outlined. Bracket indicates prosensory domain. * indicates shift of prosensory nuclei away from the luminal surface of the epithelium. N, neural side. See whole mount cochlear duct schematic (upper right) for relative positions of the serial sections. Note: unlike in Figure 7, we have switched the placement of images from *Fgf20*$^{-/-}$;*Sox2*$^{Ysb/+}$ and *Fgf20*$^{+/-}$;*Sox2*$^{Ysb/Ysb}$ cochleae to facilitate comparison.

(C) RNA in situ hybridization for *Hey1* and *Hey2* on sections through the middle turn of E14.5 *Fgf20*$^{+/-}$ and *Fgf20*$^{-/-}$ cochleae.

(D) Immunofluorescence for Myo6 (red) on “mid-modiolar” sections through the E14.5 *Fgf20*$^{+/-}$ and *Fgf20*$^{-/-}$ cochleae, with magnification. Arrows indicate Myo6-expressing hair cells. DAPI, nuclei (blue).

OS, outer sulcus; PD, prosensory domain; KO, Kölliker’s organ. Scale bar, 100 µm. See also Figure 8—Figure supplement 1.

Figure 9. *Sox2* and *Fgf20* interact to modulate a temporal buffer between specification and differentiation

Model of the roles of *Sox2* and *Fgf20* in organ of Corti development, which occurs in two stages: unspecified progenitors (tan shading) undergo specification and cell cycle exit to become prosensory cells (green shading), which then differentiate into hair cells and supporting cells (HCs & SCs; red shading). In wildtype cochleae, cell cycle exit (indicating completion of specification) begins at the apex of the cochlea and proceeds basally. Afterwards, differentiation initiates at the mid-base of the cochlea and proceeds basally and apically. Temporal buffer (green shading), which is narrow at the basal end of the cochlea but wide at the apical end, refers to the time between cell cycle exit and initiation of differentiation. In *Sox2*/*Fgf20* mutant cochleae, decrease in levels of *Sox2* expression in the developing cochlea leads to delayed prosensory specification (arrow 1), while loss of *Fgf20* leads to premature differentiation due to decreased levels of *Hey1* and *Hey2* expression (arrow 2). Loss of both *Sox2* and *Fgf20* leads to narrowing of the temporal buffer between specification and differentiation, preferentially disrupting development of the organ of Corti at the basal end of the cochlear duct (crosshatch pattern).

SUPPLEMENTAL FIGURE TITLES AND LEGENDS

Figure 1—Figure supplement 1

(A-C) Quantification of length-normalized number of (A) inner hair cells (IHCs/100 µm), (B) outer hair cells (OHCs/100 µm), and (C) supporting cells (SCs/100 µm) in the basal, middle, and apical turns of P0 cochleae from *Fgf20*$^{+/-}$, *Fgf20*$^{-/-}$ *Fgfr1*$^{flox/+}$, *Fgfr1*$^{flox/-}$, *Foxg1*$^{Cre/+}$;*Fgfr1*$^{flox/+}$, and *Foxg1*$^{Cre/+}$;*Fgfr1*$^{flox/-}$ mice. *Fgf20*$^{+/-}$ and *Fgf20*$^{-/-}$ cochleae were analyzed by unpaired Student’s t test; *Fgfr1*$^{flox/+}$, *Fgfr1*$^{flox/-}$, *Foxg1*$^{Cre/+}$;*Fgfr1*$^{flox/+}$, and *Foxg1*$^{Cre/+}$;*Fgfr1*$^{flox/-}$ cochleae were analyzed by one-way ANOVA. P values shown are from the t test and ANOVA. * indicates $p < 0.05$ from Student’s t test or Tukey’s HSD (ANOVA post-hoc); n.s., not significant.

(D) Schematic showing the positions of basal, middle, and apical turns along the cochlear duct

Figure 2—Figure supplement 1

(A, B) Sections through the middle turn of E14.5 cochlear ducts from *Fgf20*$^{+/-}$, *Fgf20*$^{-/-}$, *Foxg1*$^{Cre/+}$;*Fgfr1*$^{flox/+}$, and *Foxg1*$^{Cre/+}$;*Fgfr1*$^{flox/-}$ mice. Scale bar, 100 µm. Refer to schematic below. OS, outer sulcus; PD, prosensory domain; KO, Kölliker’s organ.

(A) RNA in situ hybridization for *Etv4* and *Etv5.* The two brackets indicate *Etv4/5* expression in the outer sulcus (OS, left) and prosensory domain (PD, right; lost in *Fgf20*$^{-/-}$ and *Foxg1*$^{Cre/+}$;*Fgfr1*$^{flox/-}$ cochleae).

(B) EdU-incorporation (green). Dashed region indicates Kölliker’s organ (KO). DAPI, nuclei (blue).

Figure 3—Figure supplement 1

Quantification of length-normalized number of inner hair cells (IHCs/100 µm), outer hair cells (OHCs/100 µm), and supporting cells (SCs/100 µm) overall (along the entire cochlea; top three graphs) and in the basal, middle, and apical turns (bottom three graphs) of P0 cochleae from *Fgf20*$^{+/-}$;*ROSA*^{rtTA} (Fgf20-het), *Fgf20*$^{+/-}$;*ROSA*^{rtTA}; TRE-Fgf9-IRES-eGfp (Fgf9-OA), *Fgf20*$^{-/-}$;*ROSA*^{rtTA} (Fgf20-null), and *Fgf20*$^{-/-}$;*ROSA*^{rtTA}; TRE-Fgf9-IRES-eGfp (Fgf20-rescue) mice. Dox regimens: E13.5-E15.5, E13.5, E14.5, or E15.5. P values shown are from one-way ANOVA. * indicates $p < 0.05$ from Tukey's HSD (ANOVA post-hoc); n.s., not significant. Summarized in Figure 3C.

Figure 4—Figure supplement 1

(A-C) Quantification of length-normalized number of (A) inner hair cells (IHCs/100 µm), (B) outer hair cells (OHCs/100 µm), and (C) supporting cells (SCs/100 µm) in the basal, middle, and apical turns of P0 cochleae from *Sox2*$^{+/+}$, *Sox2*$^{Ysb/+}$, *Sox2*$^{Ysb/Ysb}$, and *Sox2*$^{Ysb/-}$ mice. P values shown are from one-way ANOVA. * indicates $p < 0.05$ from Tukey's HSD (ANOVA post-hoc); n.s., not significant.

Figure 5—Figure supplement 1

(A) Immunofluorescence for Sox2 (red) in sections through the basal, middle, and apical turns of E14.5 *Sox2*$^{Ysb/+}$ and *Sox2*$^{Ysb/-}$ cochleae.

(B) Immunofluorescence for Ki67 (red) on serial "mid-modiolar" sections through the E14.5 and E15.5 *Sox2*$^{Ysb/+}$ and *Sox2*$^{Ysb/-}$ cochleae. Brackets indicate prosensory domain. Nine sections through the length of the cochlear duct are labeled. See whole mount cochlear duct schematic (lower left) for relative positions of the sections.

DAPI, nuclei (blue). Scale bar, 100 µm.

Figure 6—Figure supplement 1

(A) Immunofluorescence for Ki67 (red) on serial "mid-modiolar" sections through the E14.5 *Fgf20*$^{+/-}$ and *Fgf20*$^{-/-}$ cochleae. Brackets indicate prosensory domain. Nine sections through the length of the cochlear duct are labeled. See whole mount cochlear duct schematic (right) for relative positions of the sections.

(B) EdU-incorporation (green) in sections through the middle turn of E14.5 *Sox2*$^{Ysb/+}$ and *Sox2*$^{Ysb/-}$ cochleae. Dashed region indicates Kölliker's organ (KO). Bracket indicates part of Kölliker's organ without EdU-incorporating cells in *Sox2*$^{Ysb/-}$ cochleae.

OS, outer sulcus; PD, prosensory domain; KO, Kölliker's organ. DAPI, nuclei (blue). Scale bar, 100 µm.

Figure 7—Figure supplement 1

(A) P values from two-way ANOVA analyzing the quantification in (B-D). The two factors analyzed are *Fgf20* (*Fgf20*$^{+/+}$, *Fgf20*$^{+/-}$, *Fgf20*$^{-/-}$) and *Sox2* (*Sox2*$^{+/+}$, *Sox2*$^{Ysb/+}$, *Sox2*$^{Ysb/Ysb}$) gene dosage. A p value < 0.05 (yellow highlight) for *Fgf20* or *Sox2* indicates that the particular factor (independent variable) has a statistically significant effect on the measurement (dependent variable). Whereas a p value < 0.05 for Interaction indicates a statistically significant interaction between the effects of the two factors on the measurement.

(B-D) Quantification of length-normalized number of (B) inner hair cells (IHCs/100 µm), (C) outer hair cells (OHCs/100 µm), and (D) supporting cells (SCs/100 µm) in the basal, middle, and apical turns of P0 cochleae from *Fgf20*$^{+/+}$;*Sox2*$^{+/+}$, *Fgf20*$^{+/+}$;*Sox2*$^{Ysb/+}$, *Fgf20*$^{+/-}$;*Sox2*$^{+/+}$, *Fgf20*$^{+/-}$;*Sox2*$^{Ysb/+}$, *Fgf20*$^{+/+}$;*Sox2*$^{Ysb/Ysb}$, *Fgf20*$^{+/-}$;*Sox2*$^{Ysb/Ysb}$, *Fgf20*$^{-/-}$;*Sox2*$^{+/+}$, *Fgf20*$^{-/-}$;*Sox2*$^{Ysb/+}$, and *Fgf20*$^{-/-}$;*Sox2*$^{Ysb/Ysb}$ mice.

(E) Results from post-hoc Tukey's HSD analyzing the quantification results in (B-D). Letters (L, I, J, O, P, S, T; representing each measurement in panels B-D) indicate a statistically significant decrease ($p < 0.05$) when comparing the row genotype against the column genotype. L, cochlear length; I, IHCs/100 µm; O, OHCs/100 µm; S, SCs/100 µm.

Figure 7—Figure supplement 2

(A) Whole mount cochlea from P0 *Fgf20*$^{+/+}$;*Sox2*$^{+/+}$, *Fgf20*$^{+/-}$;*Sox2*$^{+/+}$, *Fgf20*$^{+/+}$;*Sox2*$^{Ysb/+}$, and *Fgf20*$^{+/-}$;*Sox2*$^{Ysb/+}$ mice showing inner and outer hair cells (phalloidin, green) separated by inner pillar cells (p75NTR, red). Magnifications show the basal, middle, and apical turns of the cochlea. Scale bar, 100 µm (magnifications), 1 mm (whole); arrowheads indicate ectopic inner hair cells.

(B-F) Quantification of (B) cochlear duct length, (C) total inner hair cells (IHCs) and IHCs per 100 µm of the cochlear duct, (D) total outer hair cells (OHCs) and OHCs per 100 µm, and (E) IHCs/100 µm and (F) OHCs/100 µm in the basal, middle, and apical turns at P0. P values shown are from one-way ANOVA. * indicates $p < 0.05$ from Tukey's HSD (ANOVA post-hoc); n.s., not significant.

Figure 8—Figure supplement 1

(A) Immunofluorescence for Sox2 (red) in sections through the basal, middle, and apical turns of E14.5 *Fgf20*$^{+/-}$;*Sox2*$^{Ysb/+}$, *Fgf20*$^{-/-}$;*Sox2*$^{Ysb/+}$, *Fgf20*$^{+/-}$;*Sox2*$^{Ysb/Ysb}$, *Fgf20*$^{-/-}$;*Sox2*$^{Ysb/Ysb}$ cochleae.

(B) Immunofluorescence for Ki67 (red) on serial "mid-modiolar" sections through the E14.5 *Fgf20*$^{+/-}$;*Sox2*$^{Ysb/+}$, *Fgf20*$^{-/-}$;*Sox2*$^{Ysb/+}$, *Fgf20*$^{+/-}$;*Sox2*$^{Ysb/Ysb}$, *Fgf20*$^{-/-}$;*Sox2*$^{Ysb/Ysb}$ cochleae. Brackets indicate prosensory domain. Nine sections through the length of the cochlear duct are labeled. See whole mount cochlear duct schematic (lower left) for relative positions of the sections.

(C) EdU-incorporation (green) in sections through the middle turn of E14.5 *Fgf20*$^{+/-}$;*Sox2*$^{Ysb/+}$, *Fgf20*$^{-/-}$;*Sox2*$^{Ysb/+}$, *Fgf20*$^{+/-}$;*Sox2*$^{Ysb/Ysb}$, *Fgf20*$^{-/-}$;*Sox2*$^{Ysb/Ysb}$ cochleae. Dashed region indicates Kölliker's organ (KO).

Note: unlike in Figure 6, we have switched the placement of images from *Fgf20*$^{-/-}$;*Sox2*$^{Ysb/+}$ and *Fgf20*$^{+/-}$;*Sox2*$^{Ysb/Ysb}$ cochleae to facilitate comparison. OS, outer sulcus; PD, prosensory domain; KO, Kölliker's organ. DAPI, nuclei (blue). Scale bar, 100 µm.

Figure 1

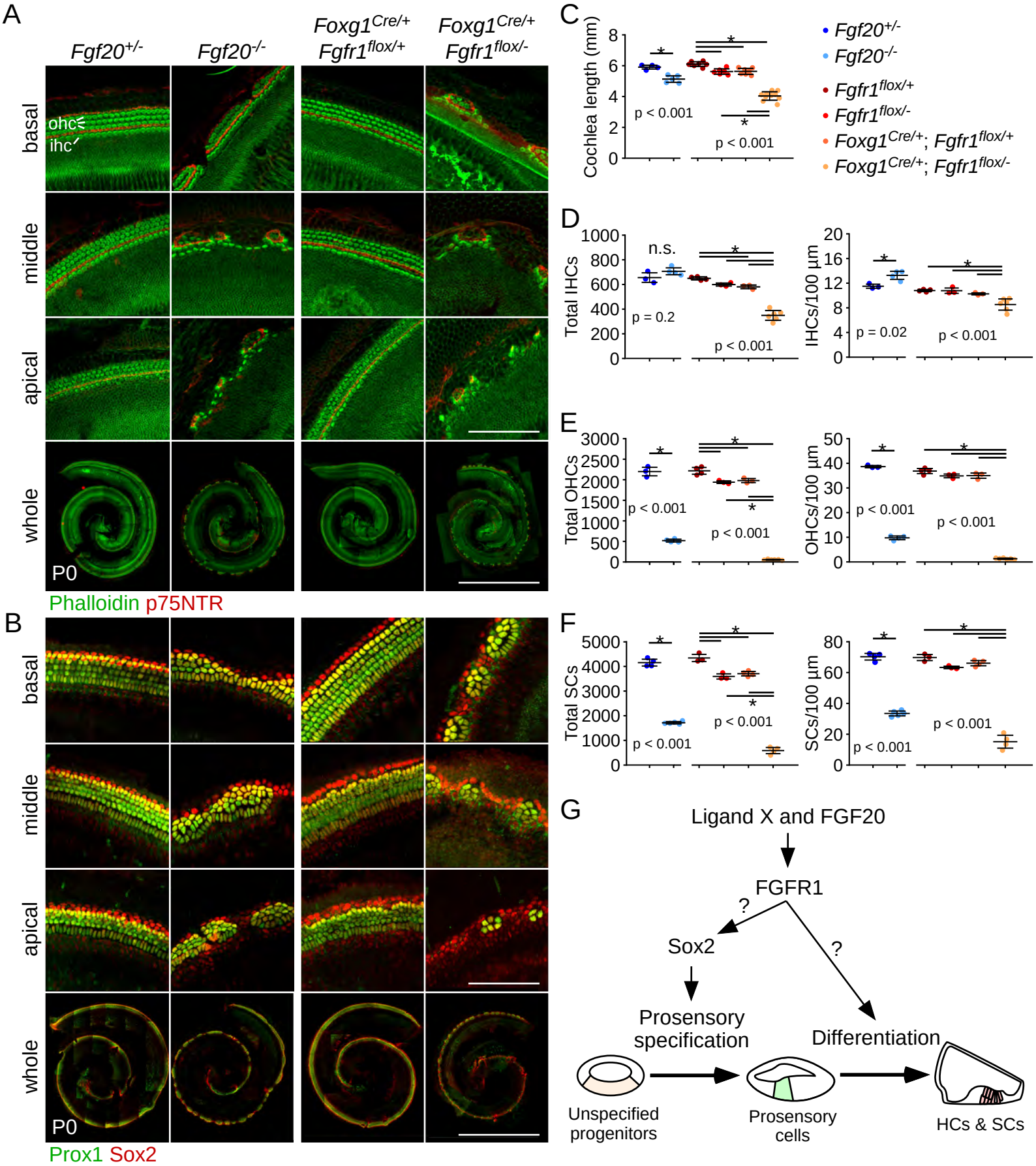
A
Fgf20+/-
Fgf20-/-
Foxg1Cre/+ Fgfr1flox/+
Foxg1Cre/+ Fgfr1flox/-
basal
middle
apical
whole
ohc
ihc
P0
Phalloidin p75NTR
B
Prox1 Sox2
C
Cochlea length (mm)
p < 0.001
Fgf20+/-
Fgf20-/-
Fgfr1flox/+
Fgfr1flox/-
Foxg1Cre/+; Fgfr1flox/+
Foxg1Cre/+; Fgfr1flox/-
D
Total IHCs
n.s.
p = 0.2
IHCs/100 µm
p = 0.02
E
Total OHCs
OHCs/100 µm
F
Total SCs
SCs/100 µm
G
Ligand X and FGF20
FGFR1
Sox2
Prosensory specification
Differentiation
Unspecified progenitors
Prosensory cells
HCs & SCs

Figure 1 supplement 1

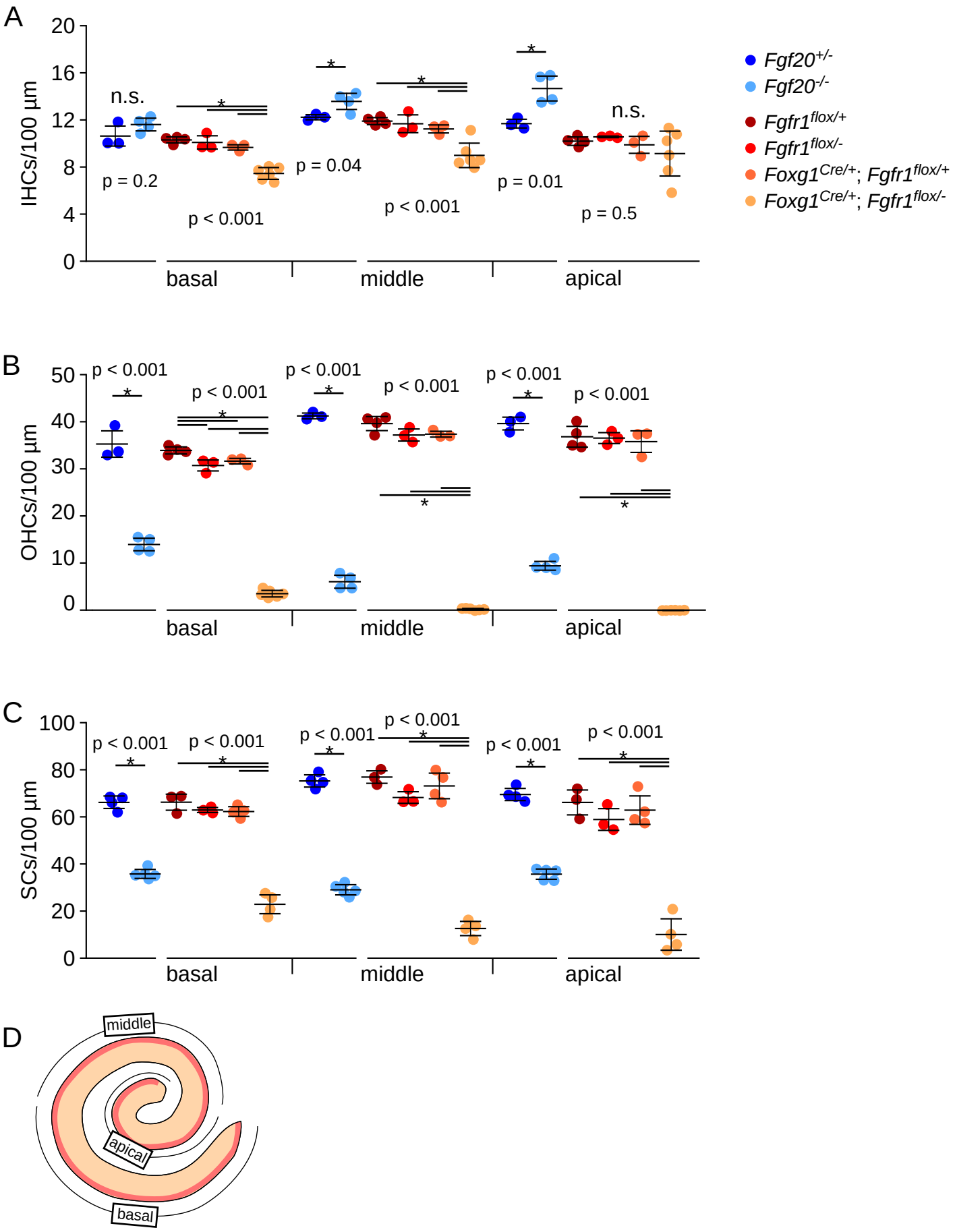

Figure 2

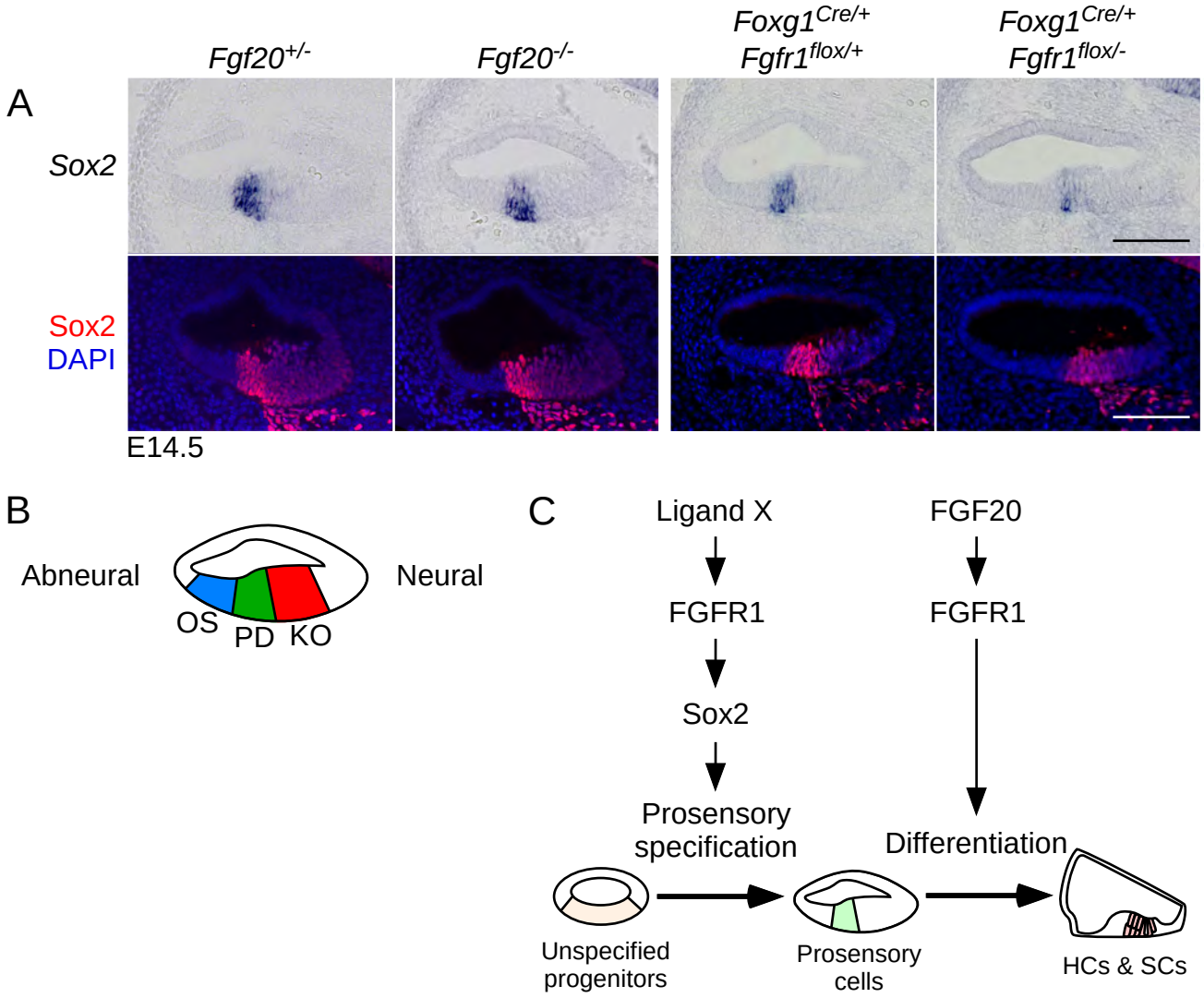
A
Fgf20+/-
Fgf20-/-
Foxg1Cre/+ Fgfr1flox/+
Foxg1Cre/+ Fgfr1flox/-
Sox2
Sox2
DAPI
E14.5
B
Abneural
Neural
OS
PD
KO
C
Ligand X
FGF20
FGFR1
FGFR1
Sox2
Prosensory specification
Differentiation
Unspecified progenitors
Prosensory cells
HCs & SCs

Figure 2 supplement 1

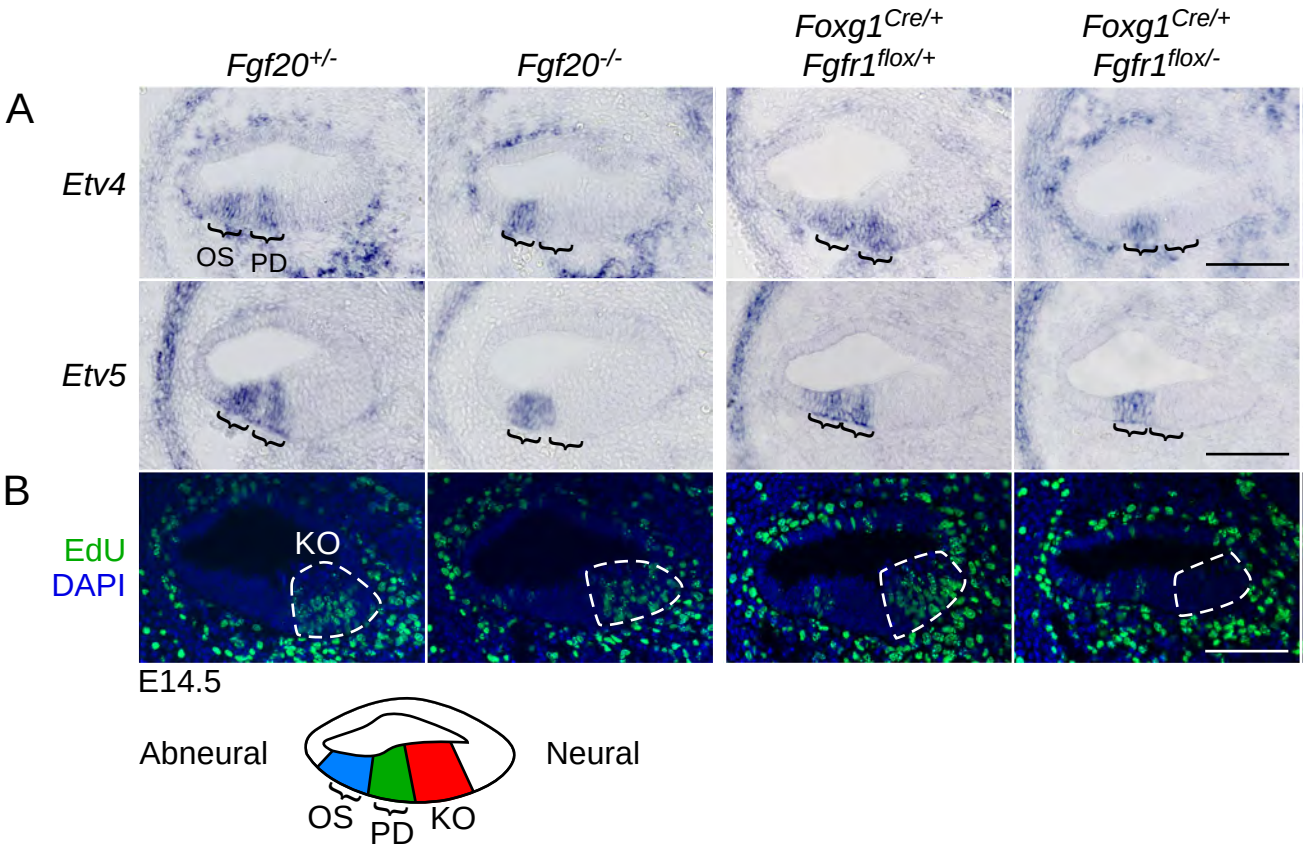

Figure 3

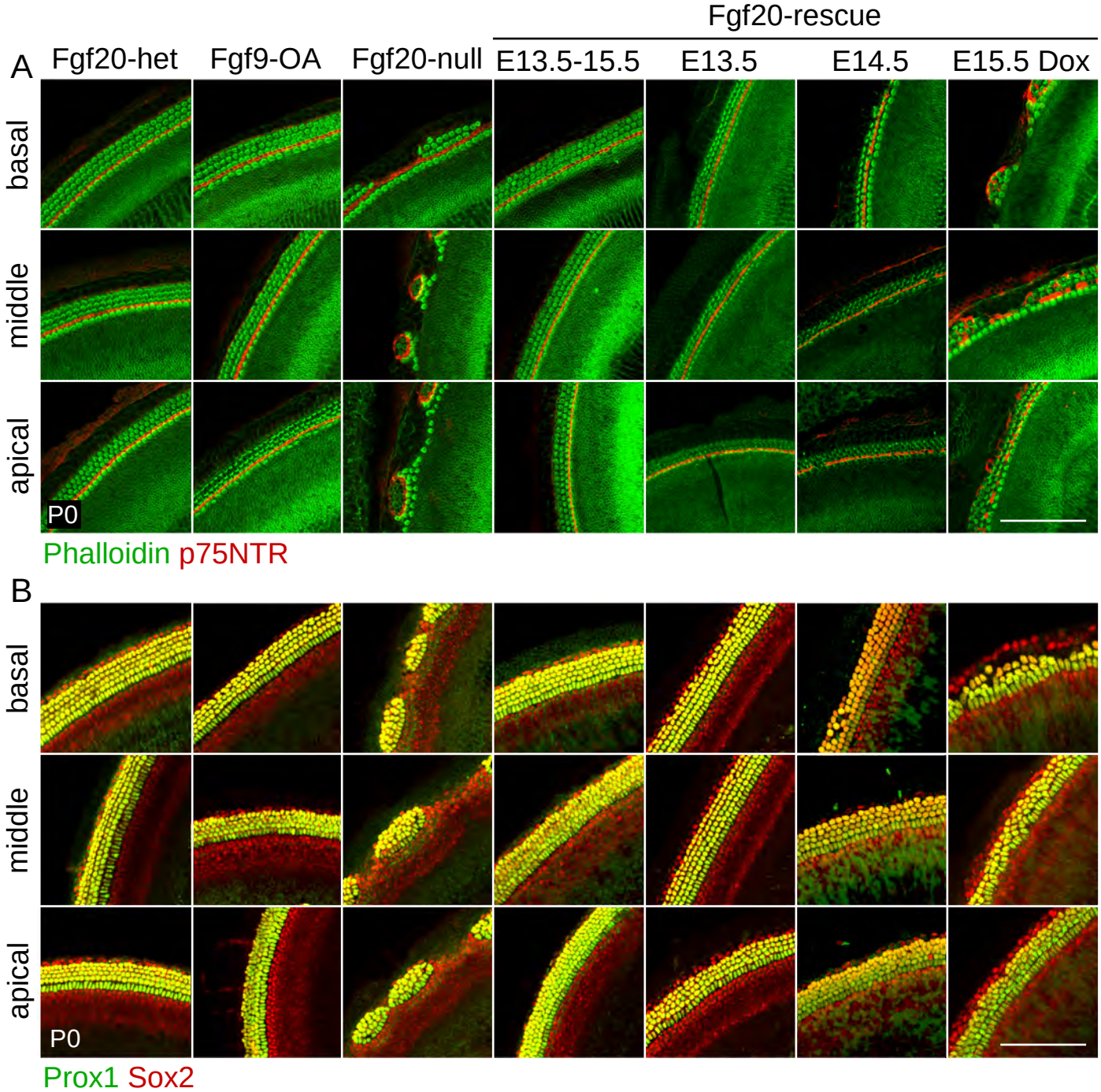

C

		Fgf9-OA	Fgf20-null	Fgf20-rescue E13.5-15.5	Fgf20-rescue E13.5	Fgf20-rescue E14.5	Fgf20-rescue E15.5 Dox
OHC	basal	95.3%*	48.6%^	105.8%*	102.4%*	76.2%*	41.7%^
	middle	99.6%*	32.4%^	108.2%*	89.0%*	94.4%*	44.7%^
	apical	97.1%*	29.0%^	101.3%*	81.2%*^	94.8%*	75.7%*^
SC	basal	99.0%*	44.1%^	103.4%*	85.6%*^	66.9%^	47.1%^
	middle	97.6%*	40.3%^	102.8%*	88.7%*	80.7%*	49.5%^
	apical	88.0%*	28.4%^	94.0%*	83.3%	74.7%	70.9%*^

<60.0%	60.0-69.9%	70.0-79.9%	80.0-89.9%	>90.0%

Figure 3 supplement 1

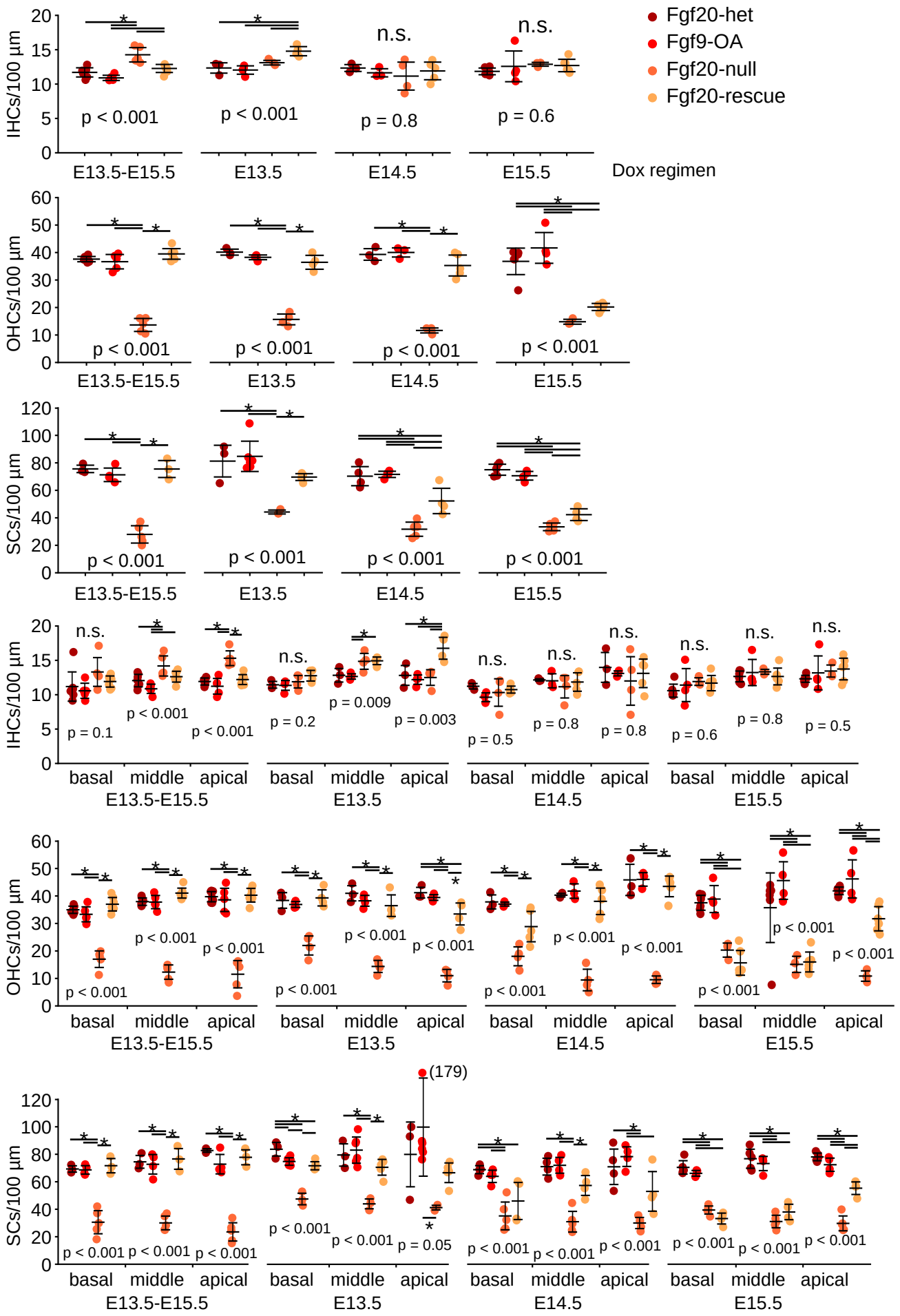

Figure 4

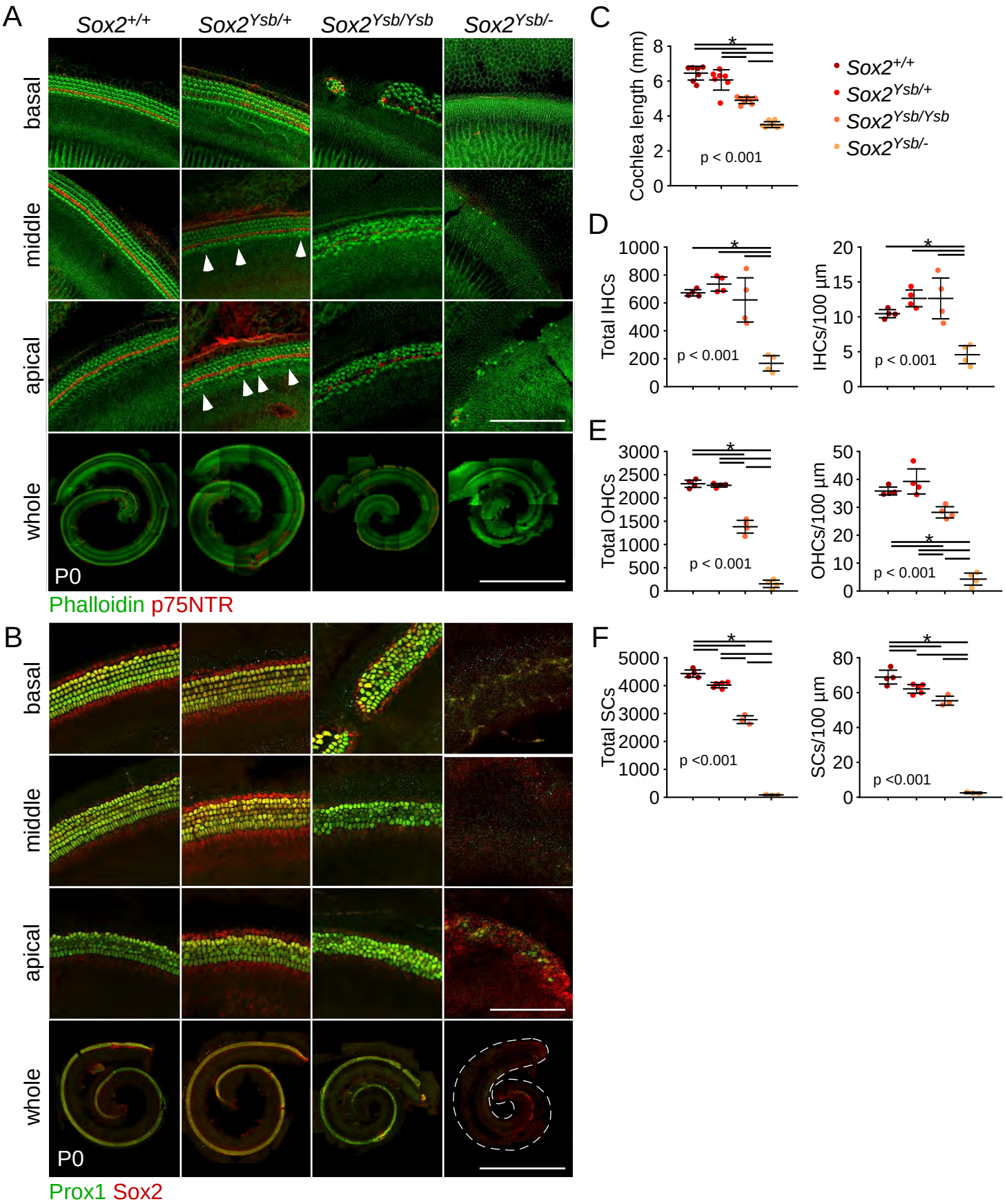
A
Sox2+/+
Sox2Ysb/+
Sox2Ysb/Ysb
Sox2Ysb/-
basal
middle
apical
whole
P0
Phalloidin p75NTR
B
basal
middle
apical
whole
P0
Prox1 Sox2
C
Cochlea length (mm)
p < 0.001
Sox2+/+
Sox2Ysb/+
Sox2Ysb/Ysb
Sox2Ysb/-
D
Total IHCs
p < 0.001
IHCs/100 µm
p < 0.001
E
Total OHCs
p < 0.001
OHCs/100 µm
p < 0.001
F
Total SCs
p <0.001
SCs/100 µm
p <0.001

Figure 4 supplement 1

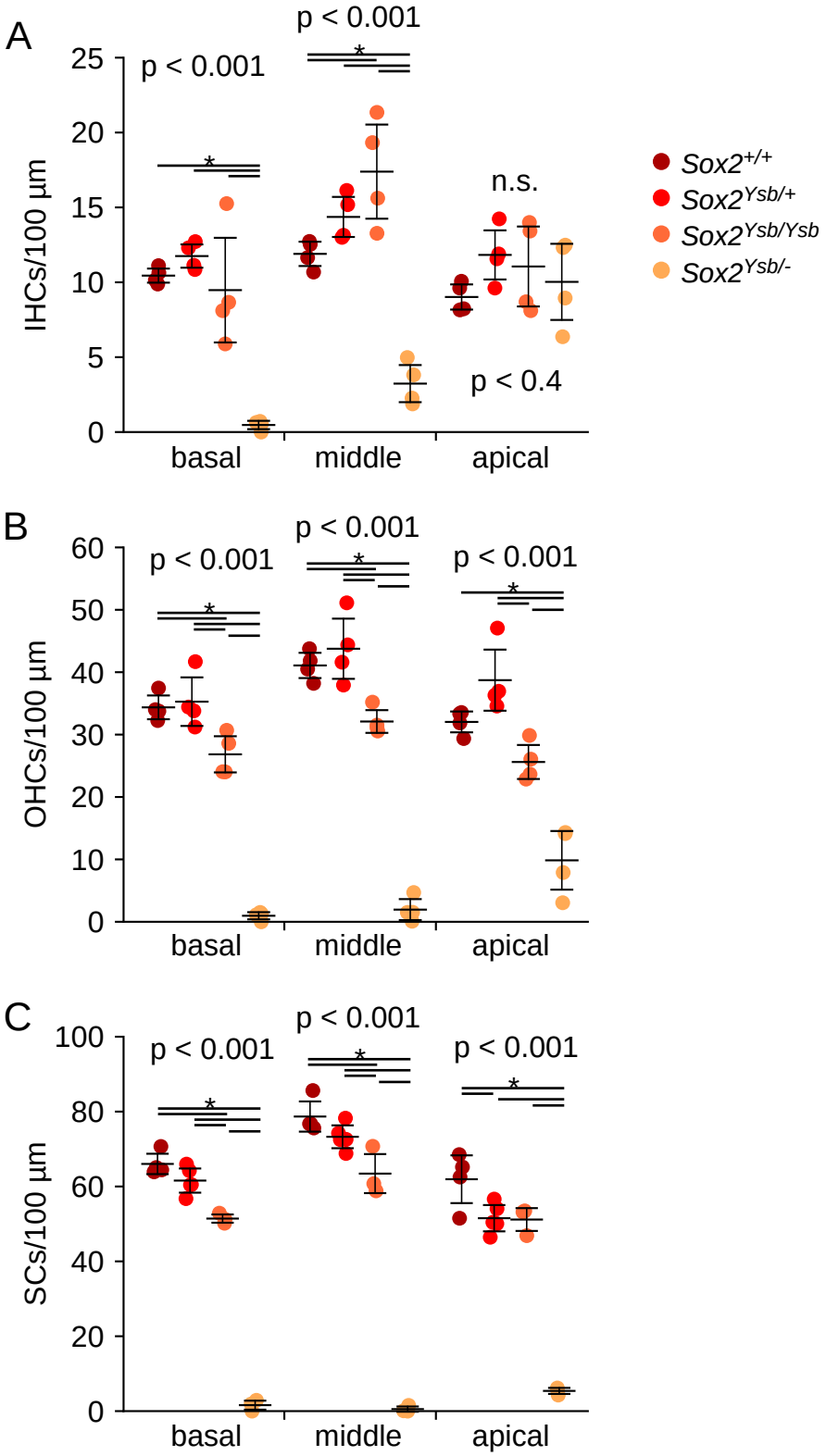

Figure 5

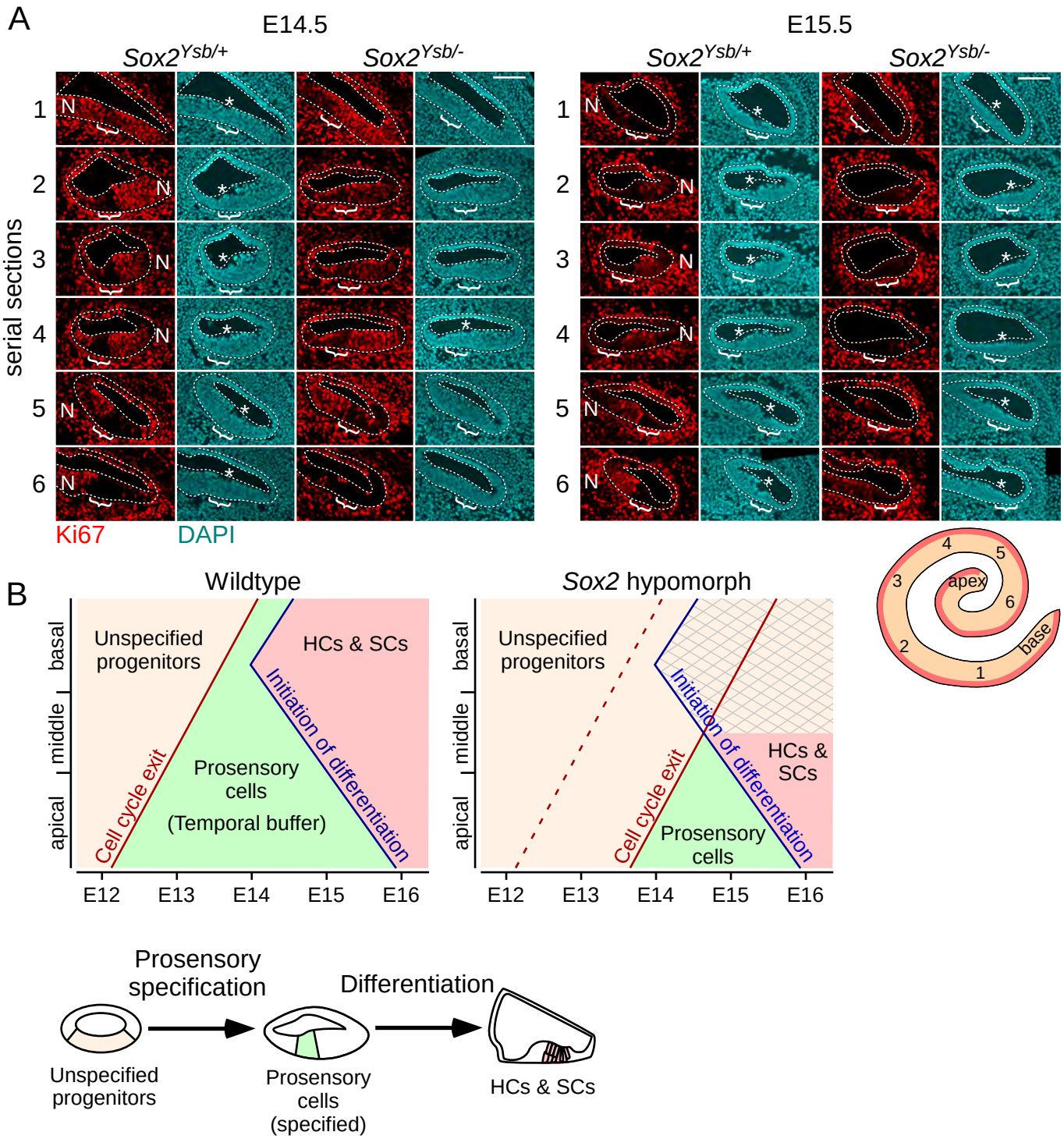
A
E14.5
E15.5
Sox2Ysb/+
Sox2Ysb/-
serial sections
1
2
3
4
5
6
N
Ki67
DAPI
B
Wildtype
Sox2 hypomorph
basal
middle
apical
Unspecified progenitors
HCs & SCs
Prosensory cells
(Temporal buffer)
Cell cycle exit
Initiation of differentiation
E12
E13
E14
E15
E16
apex
base
Prosensory specification
Differentiation
Unspecified progenitors
Prosensory cells (specified)
HCs & SCs

Figure 5 supplement 1

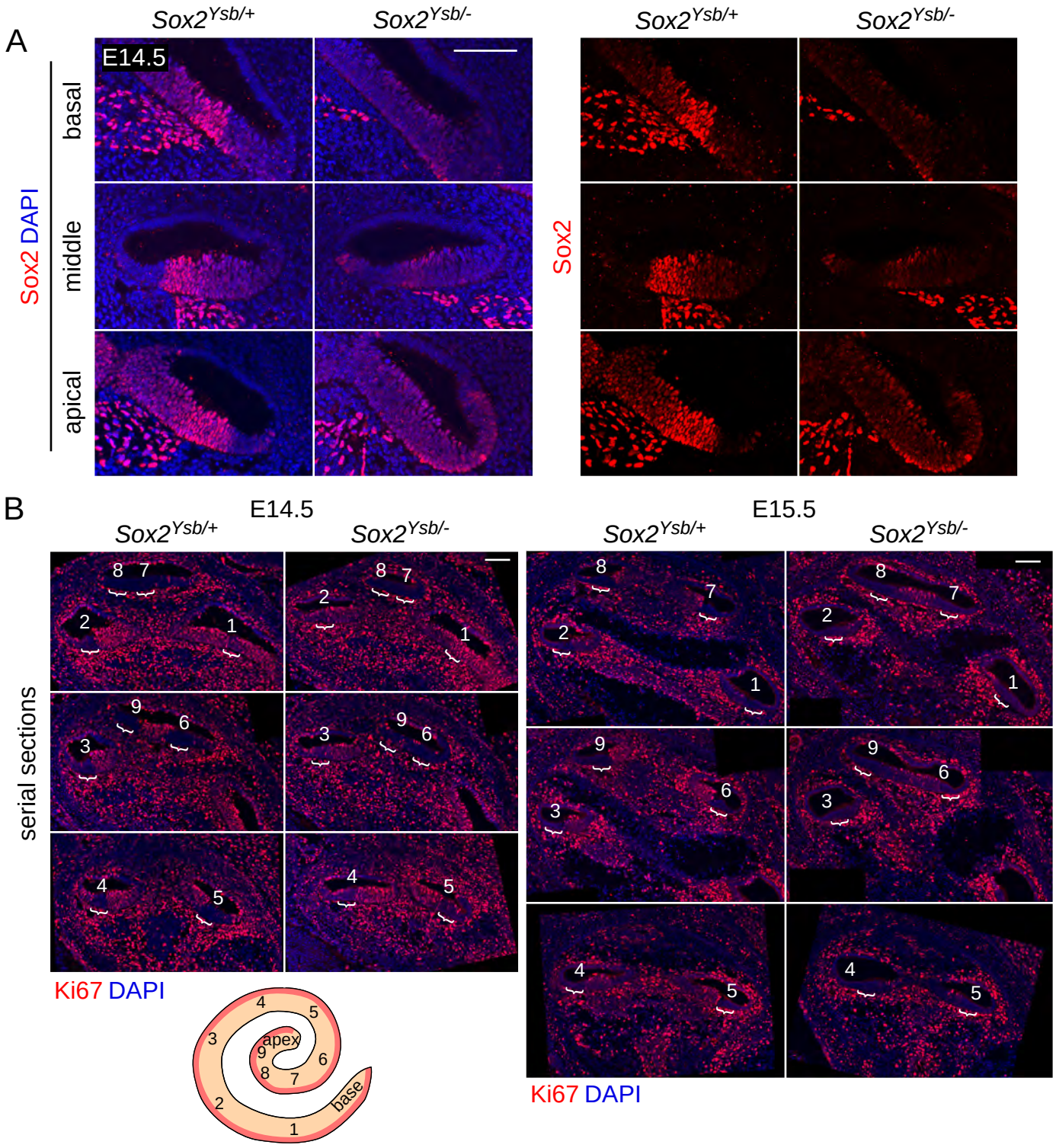

Figure 6

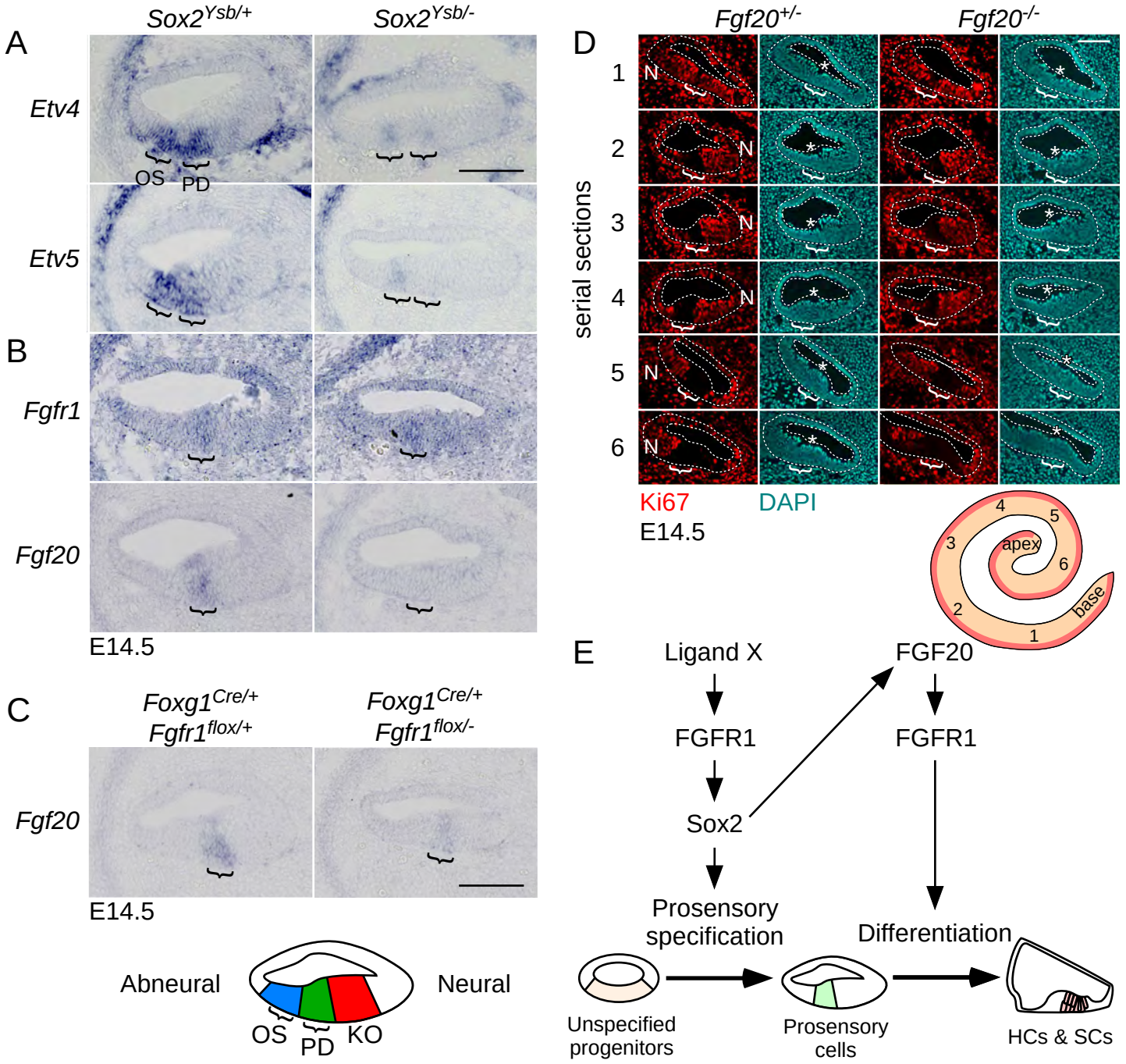
A
Sox2Ysb/+
Sox2Ysb/-
Etv4
Etv5
OS
PD
B
Fgfr1
Fgf20
E14.5
C
Foxg1Cre/+ Fgfr1flox/+
Foxg1Cre/+ Fgfr1flox/-
Fgf20
E14.5
Abneural
Neural
OS
PD
KO
D
Fgf20+/-
Fgf20-/-
serial sections
1
2
3
4
5
6
N
Ki67
DAPI
E14.5
apex
base
E
Ligand X
FGF20
FGFR1
FGFR1
Sox2
Prosensory specification
Differentiation
Unspecified progenitors
Prosensory cells
HCs & SCs

Figure 6 supplement 1

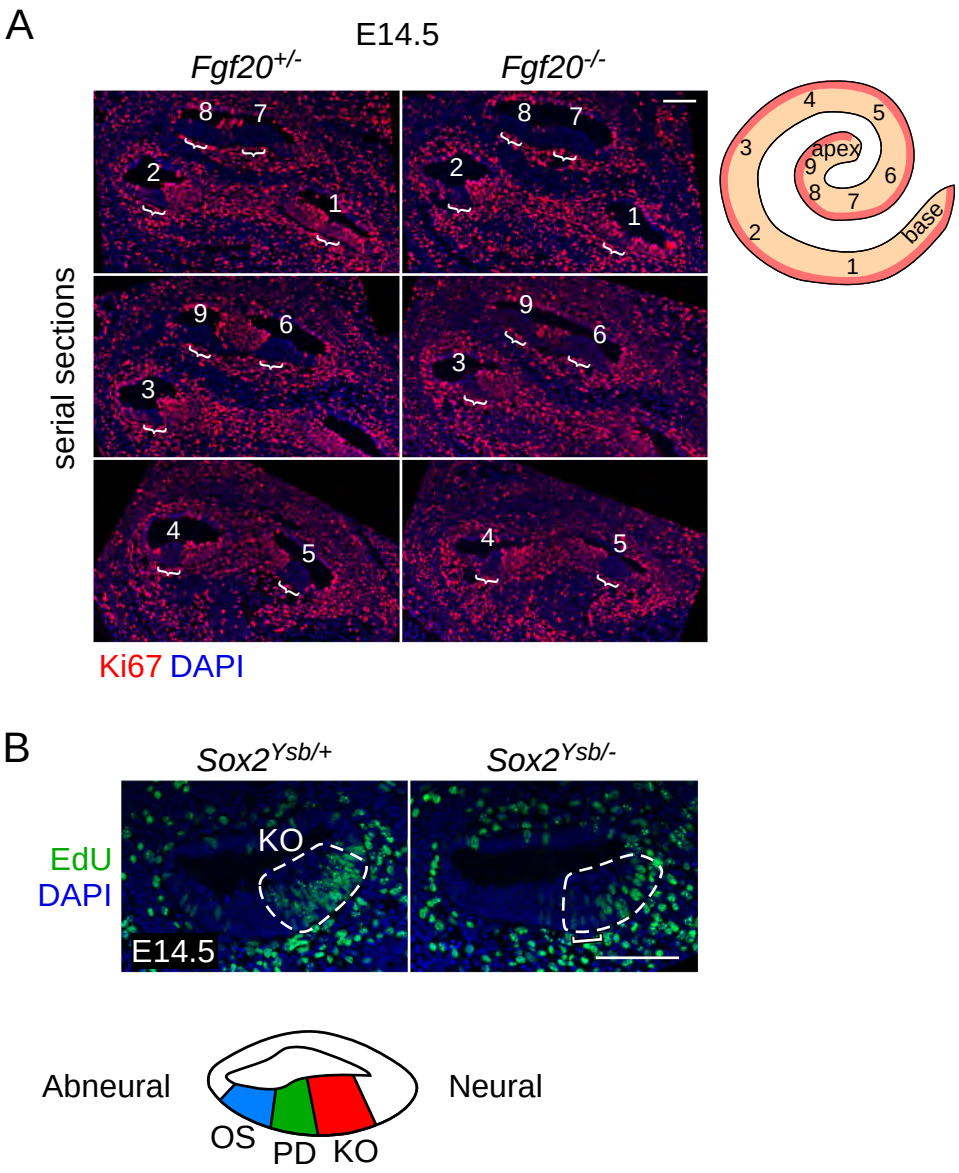

Figure 7, part I

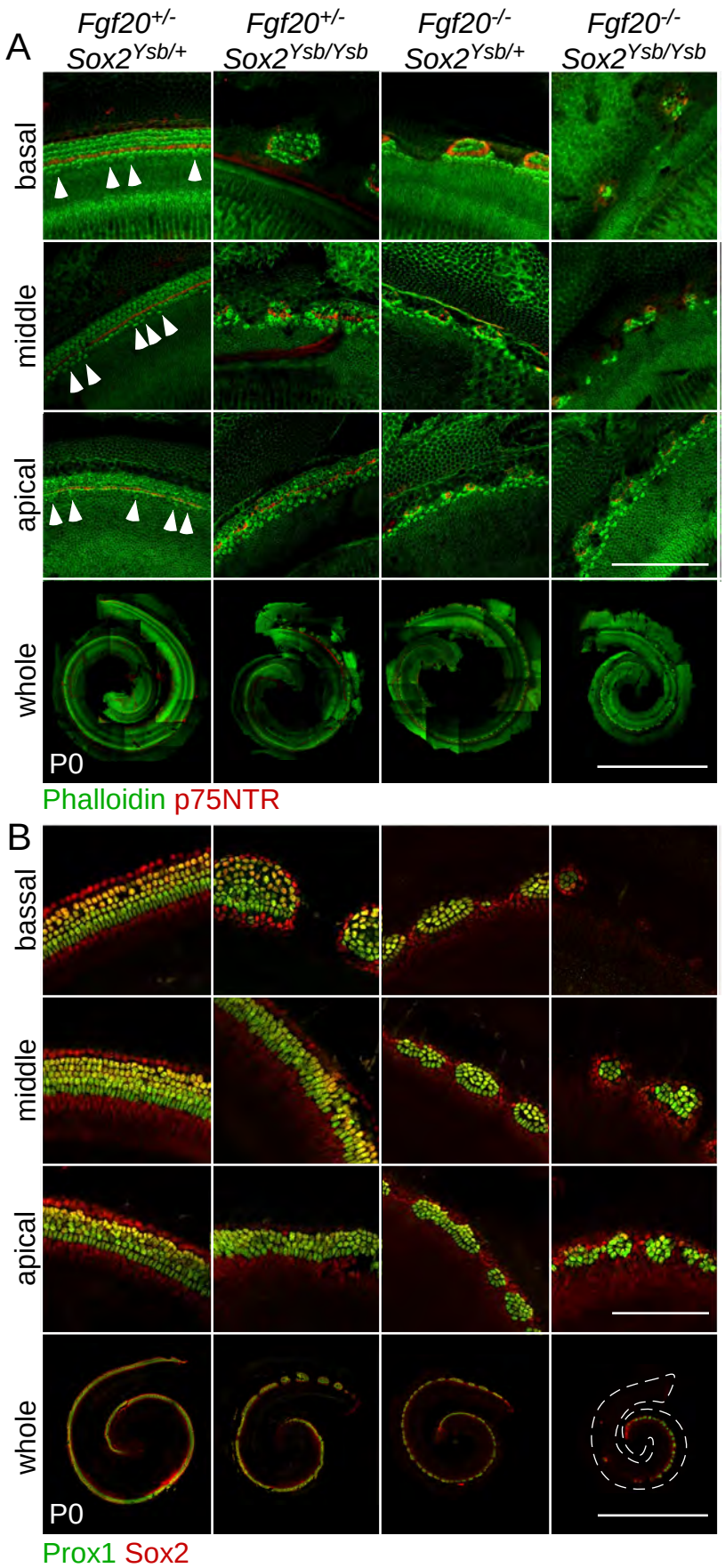

C

2-wayANOVA	*Fgf20*	*Sox2*	Interaction
Length	p < 0.001	p < 0.001	p = 0.03
Total IHC	p < 0.001	p < 0.001	p < 0.001
IHC/100µm	p = 0.002	p = 0.2	p < 0.001
Total OHC	p < 0.001	p < 0.001	p < 0.001
OHC/100µm	p < 0.001	p < 0.001	p < 0.001
Total SC	p < 0.001	p < 0.001	p < 0.001
SC/100µm	p < 0.001	p < 0.001	p = 0.3

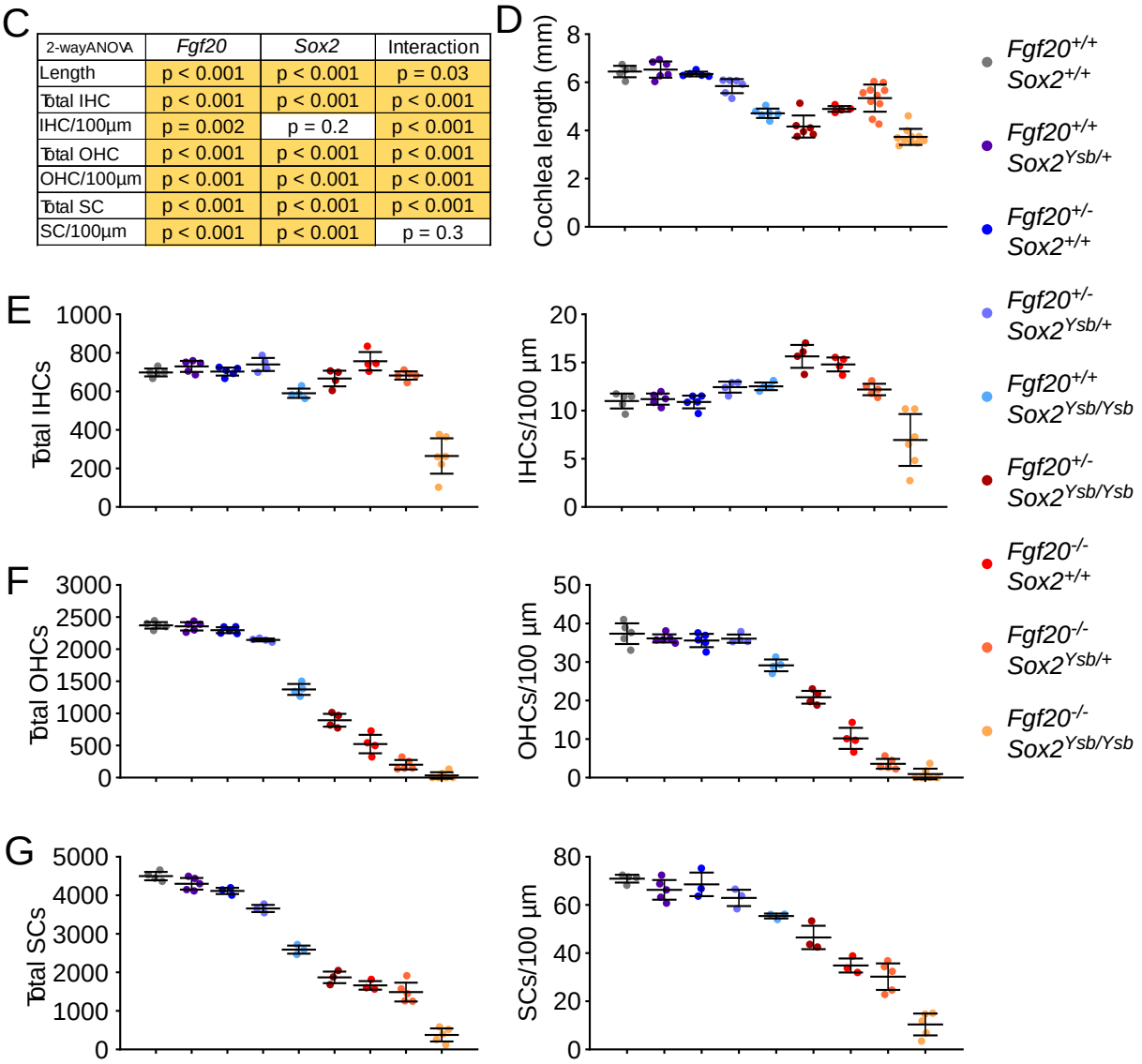

H

	Fgf20$^{+/+}$ *Sox2*$^{+/+}$	*Fgf20*$^{+/+}$ *Sox2*$^{Ysb/+}$	*Fgf20*$^{+/-}$ *Sox2*$^{+/+}$	*Fgf20*$^{+/-}$ *Sox2*$^{Ysb/+}$	*Fgf20*$^{+/+}$ *Sox2*$^{Ysb/Ysb}$	*Fgf20*$^{+/-}$ *Sox2*$^{Ysb/Ysb}$	*Fgf20*$^{-/-}$ *Sox2*$^{+/+}$	*Fgf20*$^{-/-}$ *Sox2*$^{Ysb/+}$	*Fgf20*$^{-/-}$ *Sox2*$^{Ysb/Ysb}$
Fgf20$^{+/+}$; *Sox2*$^{+/+}$						J	J		
Fgf20$^{+/+}$; *Sox2*$^{Ysb/+}$						J	J		
Fgf20$^{+/-}$; *Sox2*$^{+/+}$						J	J		
Fgf20$^{+/-}$; *Sox2*$^{Ysb/+}$	O S	O S							
Fgf20$^{+/+}$; *Sox2*$^{Ysb/Ysb}$	L OPST	L I OPS	L I OPST	L I OPS			I		
Fgf20$^{+/-}$; *Sox2*$^{Ysb/Ysb}$	L OPST	L OPST	L OPST	L OPST	OPS			L	
Fgf20$^{-/-}$; *Sox2*$^{+/+}$	L OPST	L OPST	L OPST	L OPST	OPST	OP			
Fgf20$^{-/-}$; *Sox2*$^{Ysb/+}$	L OPST	L OPST	L OPST	L OPST	OPST	JOP T	OP		
Fgf20$^{-/-}$; *Sox2*$^{Ysb/Ysb}$	L I JOPST	L I JOPST	L I JOPST	L I JOPST	L I JOPST	I JOPST	L I JOPST	L I J ST	

Figure 7 supplement 1, part I

A

2-way ANOVA	*Fgf20*			*Sox2*			Interaction		
	basal	middle	apical	basal	middle	apical	basal	middle	apical
IHC	p < 0.001	p < 0.001	p = 0.2	p < 0.001	p = 0.2	p = 0.01	p < 0.001	p < 0.001	p < 0.001
OHC	p < 0.001	p < 0.001	p < 0.001	p < 0.001	p < 0.001	p < 0.001	p = 0.002	p = 0.002	p < 0.001
SC	p < 0.001	p < 0.001	p < 0.001	p < 0.001	p < 0.001	p < 0.001	p = 0.01	p = 0.01	p = 0.7

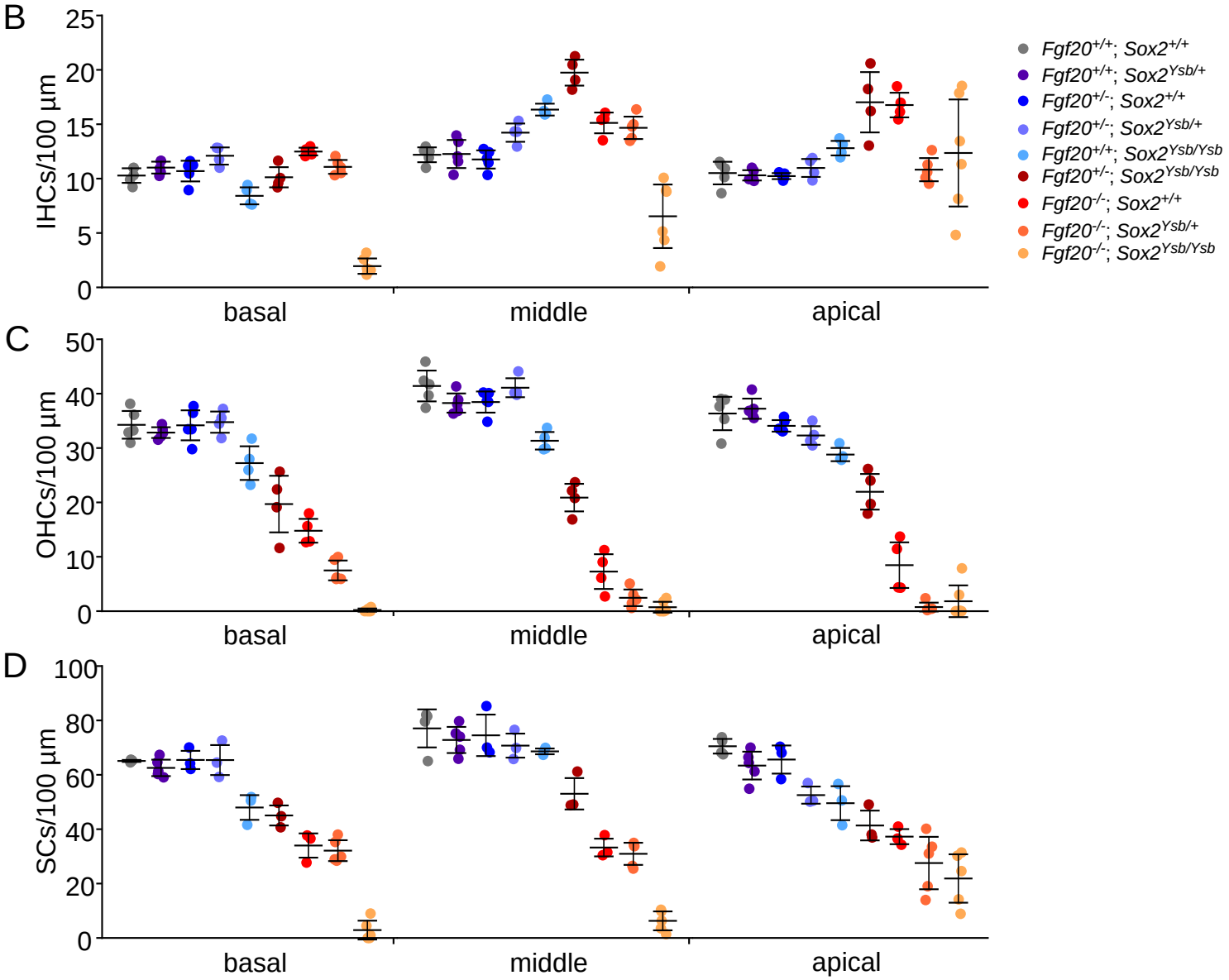

E

basal	*Fgf20*$^{+/+}$ *Sox2*$^{+/+}$	*Fgf20*$^{+/+}$ *Sox2*$^{Ysb/+}$	*Fgf20*$^{+/-}$ *Sox2*$^{+/+}$	*Fgf20*$^{+/-}$ *Sox2*$^{Ysb/+}$	*Fgf20*$^{+/+}$ *Sox2*$^{Ysb/Ysb}$	*Fgf20*$^{+/-}$ *Sox2*$^{Ysb/Ysb}$	*Fgf20*$^{-/-}$ *Sox2*$^{+/+}$	*Fgf20*$^{-/-}$ *Sox2*$^{Ysb/+}$	*Fgf20*$^{-/-}$ *Sox2*$^{Ysb/Ysb}$
Fgf20$^{+/+}$; *Sox2*$^{+/+}$				I			I		
Fgf20$^{+/+}$; *Sox2*$^{Ysb/+}$									
Fgf20$^{+/-}$; *Sox2*$^{+/+}$									
Fgf20$^{+/-}$; *Sox2*$^{Ysb/+}$									
Fgf20$^{+/+}$; *Sox2*$^{Ysb/Ysb}$	I O S	I S	I O S	I O S			I	I	
Fgf20$^{+/-}$; *Sox2*$^{Ysb/Ysb}$	O S	O S	O S	I O S	O		I		
Fgf20$^{-/-}$; *Sox2*$^{+/+}$	O S	O S	O S	O S	O S				
Fgf20$^{-/-}$; *Sox2*$^{Ysb/+}$	O S	O S	O S	O S	O S	O S	O		
Fgf20$^{-/-}$; *Sox2*$^{Ysb/Ysb}$	I O S	I O S	I O S	I O S	I O S	I O S	I O S	I O S	

middle	*Fgf20*$^{+/+}$ *Sox2*$^{+/+}$	*Fgf20*$^{+/+}$ *Sox2*$^{Ysb/+}$	*Fgf20*$^{+/-}$ *Sox2*$^{+/+}$	*Fgf20*$^{+/-}$ *Sox2*$^{Ysb/+}$	*Fgf20*$^{+/+}$ *Sox2*$^{Ysb/Ysb}$	*Fgf20*$^{+/-}$ *Sox2*$^{Ysb/Ysb}$	*Fgf20*$^{-/-}$ *Sox2*$^{+/+}$	*Fgf20*$^{-/-}$ *Sox2*$^{Ysb/+}$	*Fgf20*$^{-/-}$ *Sox2*$^{Ysb/Ysb}$
Fgf20$^{+/+}$; *Sox2*$^{+/+}$					I	I			
Fgf20$^{+/+}$; *Sox2*$^{Ysb/+}$					I	I			
Fgf20$^{+/-}$; *Sox2*$^{+/+}$					I	I			
Fgf20$^{+/-}$; *Sox2*$^{Ysb/+}$						I			
Fgf20$^{+/+}$; *Sox2*$^{Ysb/Ysb}$	O	O	O	O					
Fgf20$^{+/-}$; *Sox2*$^{Ysb/Ysb}$	O S	O S	O S	O S	O				
Fgf20$^{-/-}$; *Sox2*$^{+/+}$	O S	O S	O S	O S	O S	I O S			
Fgf20$^{-/-}$; *Sox2*$^{Ysb/+}$	O S	O S	O S	O S	O S	I O S			
Fgf20$^{-/-}$; *Sox2*$^{Ysb/Ysb}$	I O S	I O S	I O S	I O S	I O S	I O S	I O S	I S	

apical	*Fgf20*$^{+/+}$ *Sox2*$^{+/+}$	*Fgf20*$^{+/+}$ *Sox2*$^{Ysb/+}$	*Fgf20*$^{+/-}$ *Sox2*$^{+/+}$	*Fgf20*$^{+/-}$ *Sox2*$^{Ysb/+}$	*Fgf20*$^{+/+}$ *Sox2*$^{Ysb/Ysb}$	*Fgf20*$^{+/-}$ *Sox2*$^{Ysb/Ysb}$	*Fgf20*$^{-/-}$ *Sox2*$^{+/+}$	*Fgf20*$^{-/-}$ *Sox2*$^{Ysb/+}$	*Fgf20*$^{-/-}$ *Sox2*$^{Ysb/Ysb}$
Fgf20$^{+/+}$; *Sox2*$^{+/+}$						I	I		
Fgf20$^{+/+}$; *Sox2*$^{Ysb/+}$						I	I		
Fgf20$^{+/-}$; *Sox2*$^{+/+}$						I	I		
Fgf20$^{+/-}$; *Sox2*$^{Ysb/+}$						I	I		
Fgf20$^{+/+}$; *Sox2*$^{Ysb/Ysb}$	O S	O							
Fgf20$^{+/-}$; *Sox2*$^{Ysb/Ysb}$	O S	O S	O S	O	O				
Fgf20$^{-/-}$; *Sox2*$^{+/+}$	O S	O S	O S	O	O	O			
Fgf20$^{-/-}$; *Sox2*$^{Ysb/+}$	O S	O S	O S	O S	O S	I O	I O		
Fgf20$^{-/-}$; *Sox2*$^{Ysb/Ysb}$	O S	O S	O S	O S	O S	O S	O		

Figure 7 supplement 2

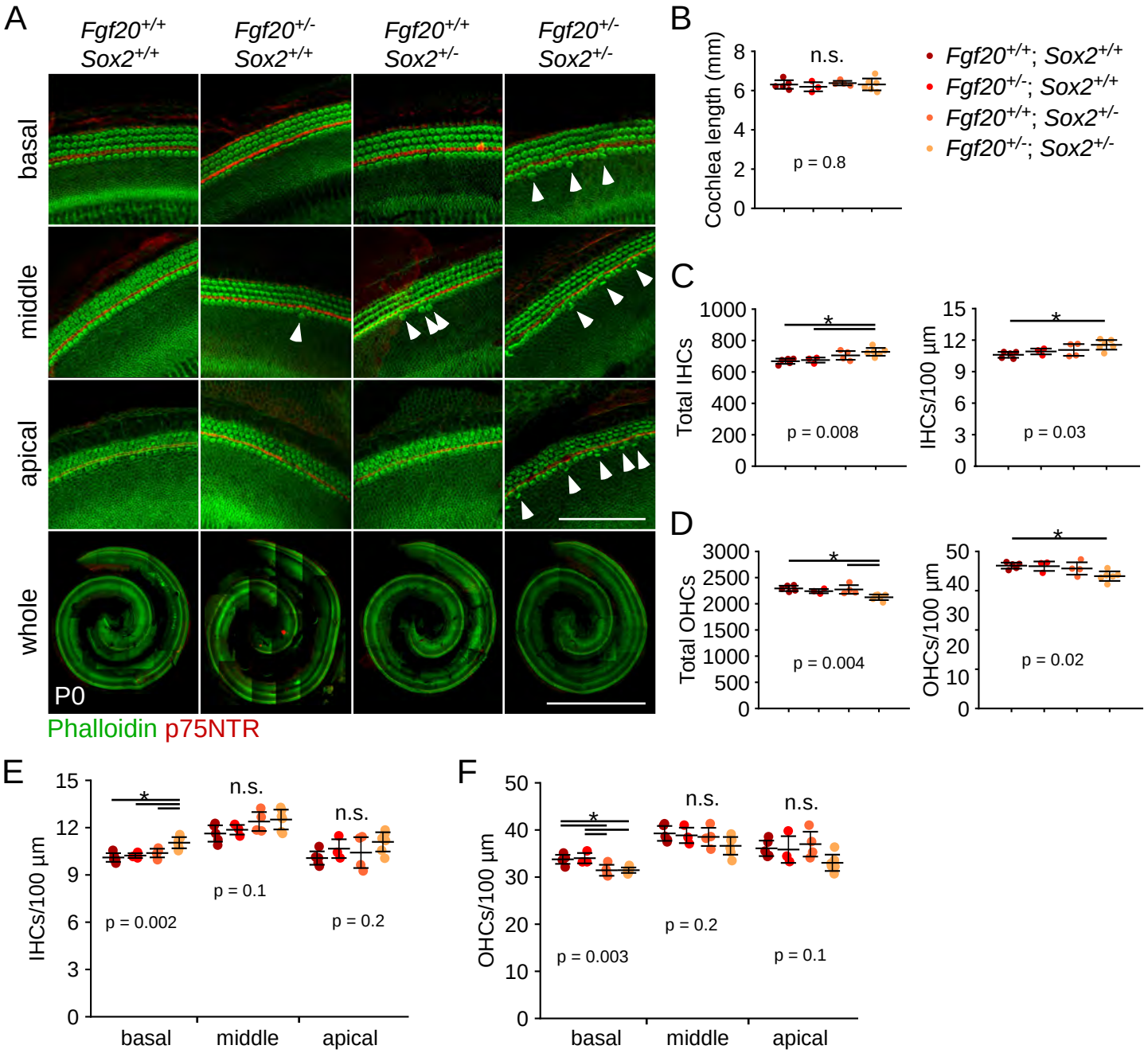

Figure 8

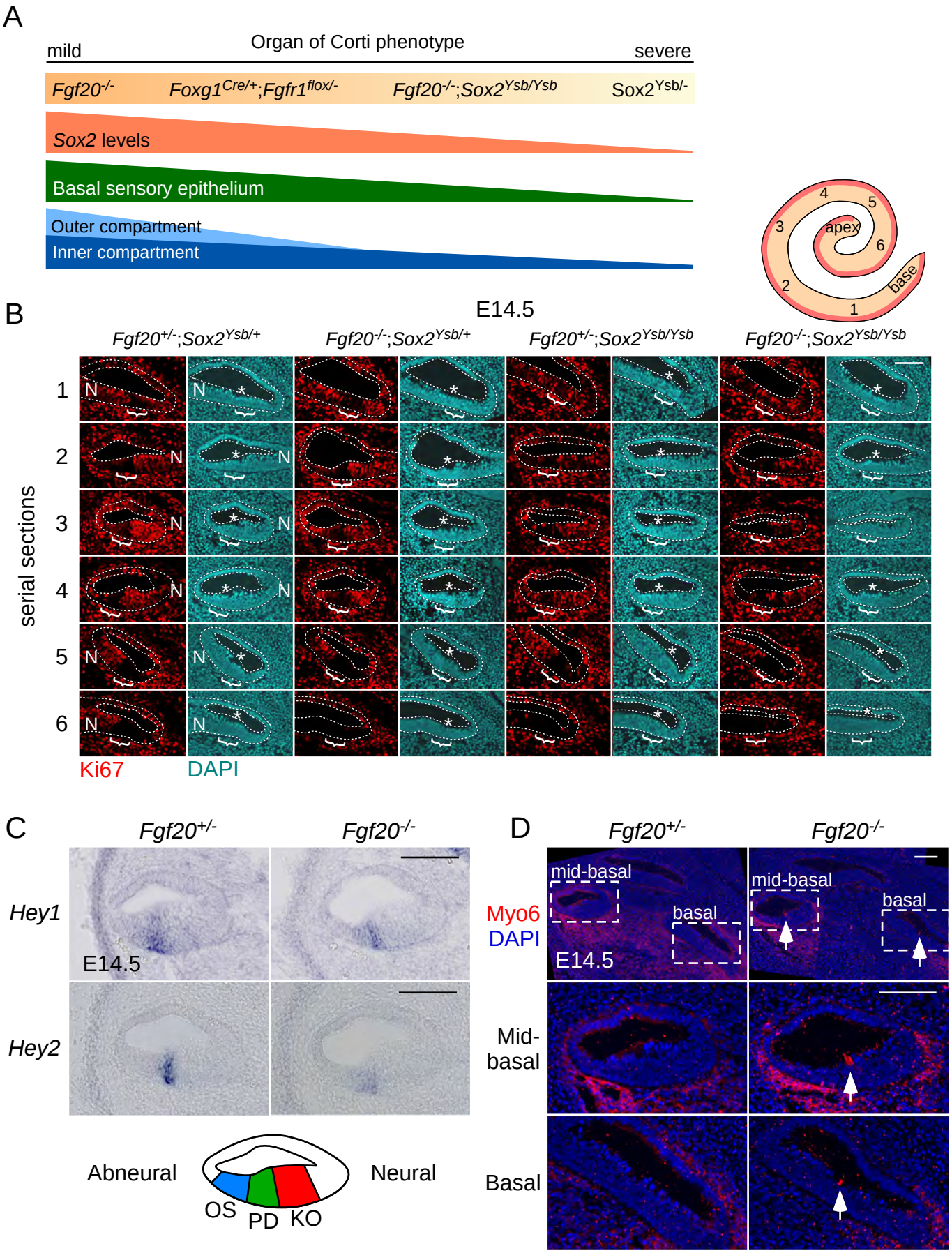
A
mild
Organ of Corti phenotype
severe
Fgf20-/-
Foxg1Cre/+;Fgfr1flox/-
Fgf20-/-;Sox2Ysb/Ysb
Sox2Ysb/-
Sox2 levels
Basal sensory epithelium
Outer compartment
Inner compartment
apex
base
1
2
3
4
5
6
B
E14.5
Fgf20+/-;Sox2Ysb/+
Fgf20-/-;Sox2Ysb/+
Fgf20+/-;Sox2Ysb/Ysb
Fgf20-/-;Sox2Ysb/Ysb
serial sections
N
Ki67
DAPI
C
Fgf20+/-
Fgf20-/-
Hey1
Hey2
E14.5
Abneural
Neural
OS
PD
KO
D
Fgf20+/-
Fgf20-/-
Myo6
DAPI
mid-basal
basal
E14.5
Mid-basal
Basal

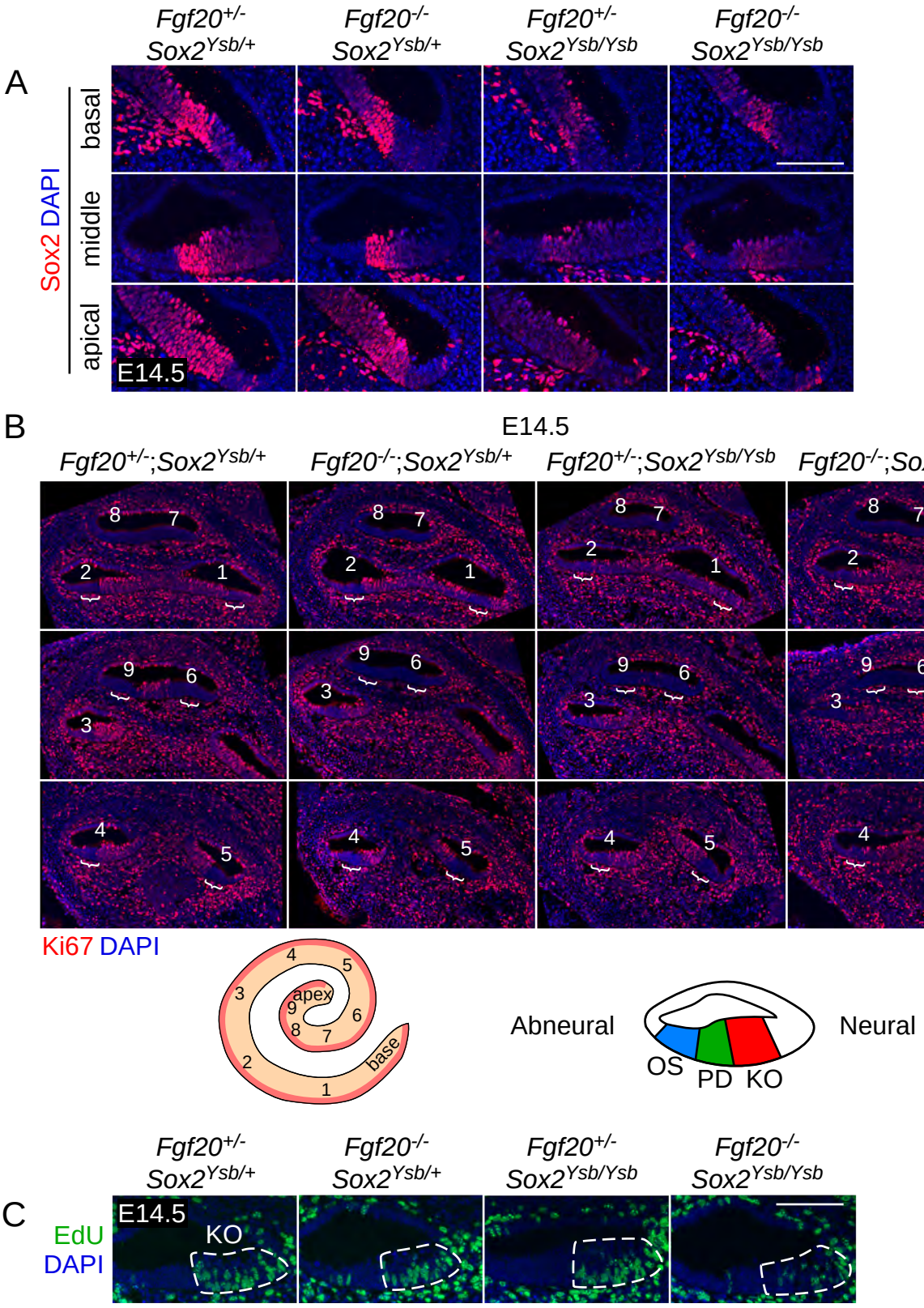
A
Fgf20+/- Sox2Ysb/+
Fgf20-/- Sox2Ysb/+
Fgf20+/- Sox2Ysb/Ysb
Fgf20-/- Sox2Ysb/Ysb
basal
middle
apical
Sox2 DAPI
E14.5
B
E14.5
Fgf20+/-;Sox2Ysb/+
Fgf20-/-;Sox2Ysb/+
Fgf20+/-;Sox2Ysb/Ysb
Fgf20-/-;Sox2Ysb/Ysb
Ki67 DAPI
apex
base
Abneural
Neural
OS
PD
KO
C
Fgf20+/- Sox2Ysb/+
Fgf20-/- Sox2Ysb/+
Fgf20+/- Sox2Ysb/Ysb
Fgf20-/- Sox2Ysb/Ysb
E14.5
KO
EdU
DAPI

Figure 9

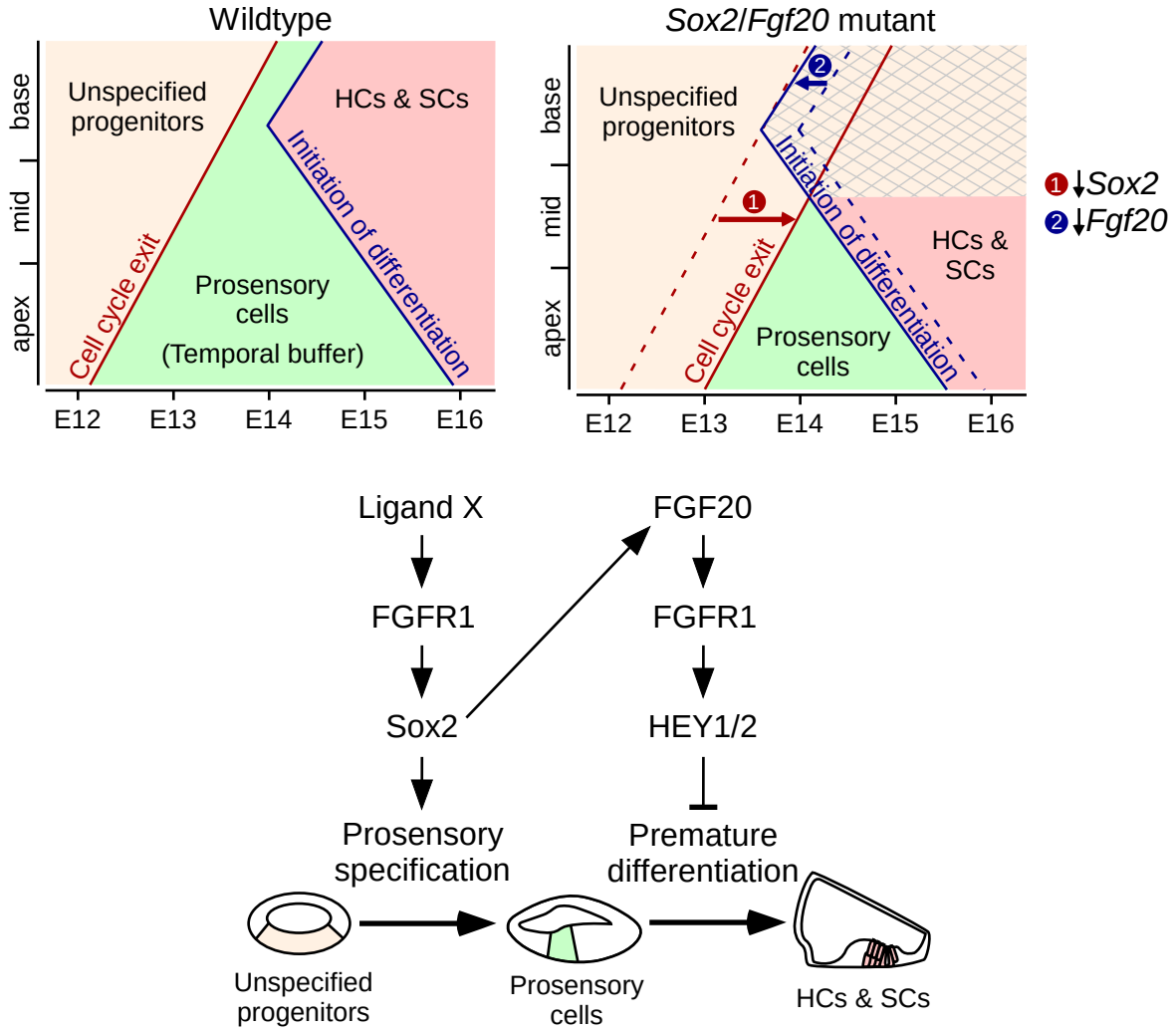
Wildtype
Sox2/Fgf20 mutant
base
mid
apex
Unspecified progenitors
HCs & SCs
Cell cycle exit
Initiation of differentiation
Prosensory cells
(Temporal buffer)
E12
E13
E14
E15
E16
❶↓Sox2
❷↓Fgf20
Ligand X
FGFR1
Sox2
FGF20
FGFR1
HEY1/2
Prosensory specification
Premature differentiation
Unspecified progenitors
Prosensory cells
HCs & SCs